Frontal Cyclogenesis

C. D. THORNCROFT AND B. J. HOSKINS

Department of Meteorology, University of Reading, Reading, England

(Manuscript received 26 October 1989, in final form 18 April 1990)

ABSTRACT

A dry baroclinic spectral model is used to study the initation of frontal cyclones in a baroclinic life cycle. The mature cyclone exhibits a frontal cyclone development associated with a finite amplitude interaction between an upper tropospheric potential vorticity (PV) cut off and a surface cold front. In comparison, a linear stability study of the front identifies only weakly growing modes at the 1000–2000 km wavelength, although with a latent heat release parameterization included in ascending regions, the baroclinic modes are considerably destabilized. It is found that the cold front in the growing baroclinic wave is in fact stabilized by the deformation present in the frontal region, an aspect neglected in studies of small amplitude perturbations to steady basic states. However, it is proposed that small scale waves often observed on the cold front baroclinicity near the warm front and seen in the life cycle experiments are the result of linear upstream development initiated by the wrap-up of low-level isotherms.

The main source of upper tropospheric PV anomalies in the atmosphere is provided by the large scale baroclinic waves which advect stratospheric air down sloping isentropes toward the surface and equator. The meridional shear present in the basic state strongly determines the nonlinear evolution of the trough, the PV advection in it, and thus the frontal cyclone developments.

1. Introduction

The understanding and forecasting of frontal cyclogenesis continues to be one of the major challenges to meteorologists. Despite rapid advances in this subject throughout the century, many storms are still poorly forecasted. Notable events include the October 1987 storm in the United Kingdom (e.g., Hoskins and Berrisford 1988) and the 1979 Presidents' Day storm in the United States (e.g., Uccellini et al. 1984). These are examples of storms that developed quickly with equivalent *e*-folding times of less than a day and had horizontal scales of order 1000 km.

Cyclogenesis and frontal cyclogenesis are somewhat vague terms. In the literature attempts are often made to separate cyclones by scale or, in work on explosive cyclones, by rate of pressure drop. The atmosphere exhibits a wide range of cyclone scales and deepening rates, and there is still no conclusive evidence that such subdivisions can be made. In discussions of frontal cyclogenesis it has become customary to separate the spectrum of cyclones into two ranges: a 3000–5000 km large-scale regime and the 1000–2000 km smaller frontal cyclone scale regime. This smaller scale is often referred to as subsynoptic or intermediate scale. Until recently, most theoretical studies have been concerned with the so-called large scale waves.

Corresponding author address: Dr. C. D. Thorncroft, Department of Meteorology, University of Reading, 2 Earley Gate, Reading RG6 2AU, England.

Using the quasi-geostrophic equations, Charney (1947) and Eady (1949) showed that baroclinic zones which are idealizations of the flows in the west Atlantic and Pacific sectors are unstable when subjected to small perturbations. With atmospheric parameters typical of the midlatitude westerlies, the most unstable wavelength is about 4000 km. Baroclinic instability theory has thus helped to explain and enhance our understanding of the large scale mobile systems that dominate our synoptic charts. The necessary conditions for instability can be discussed, as in the quasi-geostrophic work of Charney and Stern (1962), in terms of regions of opposite PV gradient (or equivalent boundary temperature gradient) and a zonal wind which is positively correlated with these gradients. This approach is made more general by considering the PV gradients on isentropic surfaces (see Hoskins et al. 1985) or theta gradients on PV surfaces (see Hoskins and Berrisford 1988). The Eady and Charney linear baroclinic instability modes are then viewed as the mathematical confirmation of the possibility of growth of a particular structure rather than as a strict representation of waves in the atmosphere.

As these large scale baroclinic waves grow into the nonlinear regime, the initially broad temperature gradients are concentrated into frontal zones (see Hoskins and West 1979), and much work has been done on two-dimensional and three-dimensional nonlinear evolution of fronts (see Hoskins 1982). The strongest gradients occur where the vertical motion is constrained, at the ground and at the tropopause. The

frontal cyclones to be discussed in this paper are those which form on these frontal zones within the large scale baroclinic wave, although particular emphasis is given to the surface frontal zones. The cyclones observed along these zones tend to have wavelengths in the 1000–2000 km range and smaller and are thus in the second region of the spectrum which has inspired interest.

The Norwegian model for frontal cyclones development of Bjerknes and Solberg (1922) describes the life cycle of a typical frontal cyclone development. Although it has continued to dominate the perception of cyclones in the Atlantic sector ever since, it does little to enhance the understanding of the initiation and growth of these systems. Most theoretical work has concentrated on the linear nonseparable eigenvalue problem, including that by Solberg (1928), Kotchin (1932), Eliasen (1960), Orlanski (1968) and more recently Moore and Peltier (1987), Joly and Thorpe (1990a), and Schär and Davies (1989). This approach assumes, as suggested by Bjerknes and Solberg (1922), that frontal cyclones will evolve from a small perturbation in the frontal zone. These authors look for rapidly growing normal modes assuming that these will evolve and dominate from a random set of initial conditions.

Frontal zones are characterized by large horizontal temperature gradients and often by large PV gradients. In the upper troposphere these are between extruded polar stratospheric air and air with low PV due to its subtropical origin or the reduction of PV associated with diabatic processes, as stressed by Thorpe and Emanuel (1985). These same diabatic processes lead to large values of PV at low levels and consequent PV gradients. The work of Cullen and Purser (1984) suggests that large tropospheric PV could also be associated with the extrusion of the boundary layer into the interior. Thus, as suggested by Thorpe and Emanuel (1985), the Charney-Stern necessary conditions for instability are satisfied by atmospheric frontal zones. The growth rate may be expected to increase with increased temperature and PV contrasts and thus, we might anticipate more vigorous growth of smaller scale systems on a stronger frontal zone. Cyclone scale type modes are found by applying the Eady model to a shallow layer of the atmosphere (e.g., Staley and Gall 1977; Harold and Browning 1969). However, from the above discussion, the Eady model, which has no interior PV gradients, is not a good representation of a realistic frontal zone.

It is usually observed that frontal cyclones have a significant amount of precipitation associated with them. Latent heat release might therefore be important in the actual cyclogenesis as well as in the formation of the ambient flow. Certainly Bosart (1981) and Reed and Albright (1986) have shown this to be true in their observational studies. The maximum Eady growth rate is inversely proportional to the buoyancy frequency N. In a moist atmosphere the effective N is reduced and larger growth rates can be anticipated. Further, the wavelength of maximum growth rate decreases with N. It is important to note that this argument ignores the asymmetry between upward and downward motion. However, in a study by Emanuel et al. (1987), with latent heat release only in the ascending air, the growth rate of the most unstable mode increased by 2.6 while the wavelength decreased by 0.6.

Another process which is often ignored in linear studies is surface drag. Farrell (1985) suggested that drag will stabilize all modes, but Valdes and Hoskins (1988) have shown that, even for the observed zonally averaged flow with its relatively weak baroclinicity, it is only the smaller scale modes that are stabilized. The shallow frontal cyclone modes identified in most of the linear studies are likely to be significantly damped by surface drag. The drag can also, however, act as a source or sink of PV and may be important in some cyclone developments.

Recently, it has been shown by Arakawa and Moorthi (1988) and Bell and White (1988) that spurious computational modes can occur in vertically discretised models. In the former study, they were associated with modes which are short enough that their natural vertical scale is comparable with the height of the lowest full level in a Lorenz-type vertical scheme. In the second study, they are associated with critical levels close to grid-levels. Preliminary work suggests that with the grid-spacing, the horizontal scales, and the explicit diffusion used here such spurious instability is not a problem. Except where stated, the results are not more dependent on the resolution or diffusive parameterization than would be anticipated by simple arguments.

It is of interest to compare some of the linear studies which have been performed. These vary in the basic states they examine and the equations used. For the frontal cyclone problem, when the scales of interest are typically about 1000 km, semigeostrophic theory may provide an adequate description, although the neglected ageostrophic momentum will become more important for smaller scales. For example, Stone (1966) repeated the stability of the Eady basic state with the primitive equations and found small scale modes beyond the Eady cut-off. The first linearized analysis, which directly addressed the frontal cyclone problem, used Margules (1906) two-fluid model of a front consisting of two uniform PV fluids with a discontinuity between them. These studies included those of Solberg (1928), Kotchin (1932), and Eliasen (1960). The most comprehensive study of a two-fluid model was carried out by Orlanski (1968). Using the primitive equations, he explored a large region of parameter space identifying several types of modes including the Eady baroclinic mode. He also identified a 1000–2000 km scale mode, which he referred to as the Bjerknes mode since he believed it to explain frontal cyclone instability. Duffy (1976) repeated Orlanski's work using the semigeostrophic equations and also found the Bjerknes mode, but with a reduced growth rate.

More recently, Moore and Peltier (1987) have stud-

ied the stability of the Hoskins and Bretherton (1972) (henceforth denoted HB) uniform PV front. Using the primitive equations they exhibited two extra modes beyond the Eady cut off, one of which they postulated to be a frontal cyclone mode. Because the HB front has uniform interior PV, the Charney Stern theorem, as extended by Hoskins (1976), allows only unstable Eady-type modes at the level of semigeostrophic theory. Thus, the Moore and Peltier (1987) modes would appear to rely on the neglected ageostrophic momentum for their existence. Indeed, Joly and Thorpe (1990a) investigated the stability of the HB front with the semigeostrophic equations and found only the Eady branch. However, for a frontal zone with interior PV gradients, the semigeostrophic equations will indeed identify other modes, as has been confirmed by Joly and Thorpe (1990a).

Another assumption in most frontal cyclogenesis studies is that the basic front is taken to be a steady solution of the governing equations. However, the deformation present in the large scale cyclone wave, which is the reason that the front forms in the first place, is likely to suppress any weak linear instability [see Juckes and McIntyre (1987)]. Joly and Thorpe (1990b) have recently managed to break new ground by looking at the growth of perturbations to a growing two-dimensional Eady mode. It is also important to recognize that fronts have a finite length and varying properties along that length. Pierrehumbert (1984) recognized similar problems in the context of large scale baroclinic instability and thus studied the stability of a zonally varying basic state. He distinguishes between global modes which rely on the cyclic nature of the domain and local modes. He concluded that from a random set of initial conditions global modes take much longer to emerge and nonlinear effects may become important before a normal mode is realized. Such a study has not been done for a frontal zone with strong horizontal and vertical wind shears but it is clear that only local modes are revelant.

In contrast to the natural selection principle where the fastest growing normal mode dominates from a random set of initial conditions, baroclinic growth seen in the western Atlantic, for example, is often found to be triggered by an upper level disturbance moving off the continent. The development resulting from the interaction of an upper level disturbance with the surface frontal region is frequently referred to as Pettersen type B cyclogenesis (see Pettersen et al. 1962; Pettersen and Smebye 1971). This nonmodal finite amplitude initiation can be thought of in terms of PV anomalies, as described by Hoskins et al. (1985). This approach does not rely on complete phase locking of Rossby waves, and growth rates greater than those predicted from linear theory can result. With this perspective, the origin of these PV anomalies must be considered. One view is that they are part of the atmospheric "debris" left over from previous events. Alternatively, they can also be provided by the parent cyclone in the form of a trough tip or cut-off. Further, Kleinschmidt (1957) stressed that cyclogenesis can be associated with PV anomalies generated by diabatic processes. Whatever the origin of the PV anomaly, the interaction with the surface baroclinicity and consequent cyclogenesis is similar.

The notion of finite amplitude nonmodal growth should also be compared with the idealized studies of Farrell (1982, 1984). He has very convincingly shown that nonmodal solutions of linearized equations can exhibit larger perturbation energy growth than a normal mode analysis would suggest. The archetypal situation for such growth is a structure similar to that considered in the PV discussion.

This paper approaches the frontal cyclone problem using the baroclinic spectral model developed by Hoskins and Simmons (1975). A triangular truncation at total wavenumber 95 (T95) is used with 30 irregularly spaced sigma levels. This gives a resolvable horizontal length scale (wavelength/2π) of about 67 km. Below about 700 mb the level spacing is everywhere less than about 23 mb, whereas above this it is close to 50 mb. The model is dry and frictionless except that an internal hyper-diffusion is added to the vorticity, divergence, and temperature tendency equations in the form of $-k\nabla^6 X$. The value of k was chosen to give a decay rate of $(1\ \text{h})^{-1}$ for the shortest retained scale. This is the only diabatic process included.

In section 2 results are presented at the present resolution for the basic baroclinic wave life cycle described by Simmons and Hoskins (1980), (hereafter denoted SH) on the basis of a T42, 15 layer calculation. A frontal cyclone development is shown to occur during the late stages of the life cycle, a development only hinted at in the earlier, lower resolution run. In section 3 the linear stability of the cold front which formed in the life cycle is examined. The analysis is performed both for the dry equations and with a crude representation of moist processes. In section 4 an alternative mechanism for frontal wave development is shown. This upstream development mechanism was originally proposed in this context by Simmons and Hoskins (1979). A final discussion is presented in section 5.

2. Baroclinic life cycle

a. Large scale view

The life cycle experiment presented here is the basic case of SH but with increased horizontal and vertical resolution. The basic zonal flow for the case is shown in Fig. 1. There is a baroclinic zone centered at about 45°N with a temperature contrast at the surface of about 35°K between 60°N and 30°N and an associated 47 m s^{-1} jet at about 300 mb. This may be considered to represent a western ocean basin wintertime situation.

The basic state is unstable and in order to investigate how this instability is realized, the nonlinear primitive equation model is initialized with the basic flow plus the most unstable normal mode at zonal wavenumber

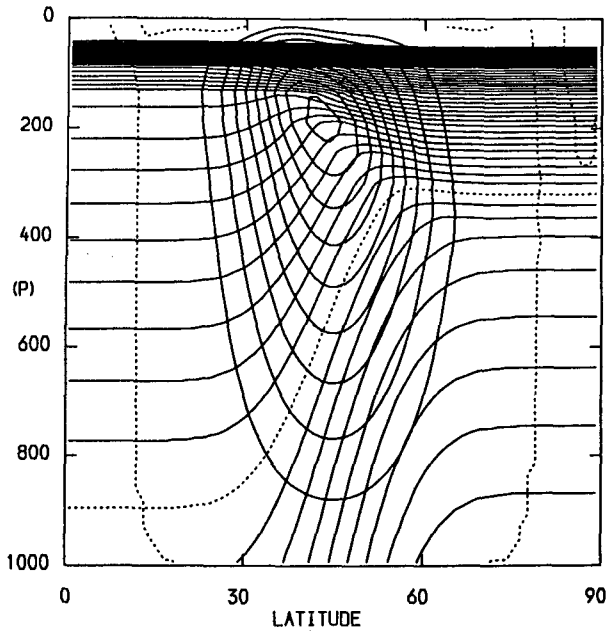

FIG. 1. Latitude-height section showing potential temperature and zonal velocity for the basic state. Potential temperature contours are drawn every 5 K with the 300 K contour dashed. Zonal velocity contours are drawn every 5 m s^{-1} with the zero contour dashed.

6 with a surface pressure perturbation of 1 mb. At 45°N this mode has a wavelength of approximately 4700 km, corresponding to the larger scale cyclones discussed above. As in the previous studies of SH, we only consider zonal wavenumber 6 and its harmonics and only one hemisphere. Although it is recognized that 6 identical cyclones developing around each hemisphere is unrealistic, considerable insight into important synoptic events is gained. Such experiments are presented as sequences of dynamical events providing a paradigm for observed events in the atmosphere.

The global energetics for the basic life cycle are shown in Fig. 2. They have been calculated using the scheme developed by Pearce (1978) which divides the available potential energy (APE) into a "static stability" part (AI) and a meridional temperature variance part (AZ). The wave grows rapidly by baroclinic conversions up to about day 7 with KE growing at the expense of the APE. After this, the wave loses energy equally rapidly to the basic state kinetic energy (KZ). Thus, the life cycle can be viewed as a wave growing by baroclinic energy conversions followed by barotropic decay. It is of interest to note that although considerably more synoptic detail is seen in this T95 30 level integration than in the T42 15 level run, the differences in peak KE reached 11.2×10^5 J m^{-2} and 9.9×10^5 J m^{-2}, respectively, and energetics in general are small.

Held and Hoskins (1985) have shown how the life cycle can be viewed in terms of upward and equatorward Rossby wave propagation after a low-level saturation event. An upper-level saturation event follows the upward propagation and the eddy is removed. Also see Edmon et al. (1980) and Karoly and Hoskins (1982) who view this propagation in terms of refractive index ideas.

Although it is important to be aware of the large scale control present in the life cycle, this paper concentrates on the smaller frontal cyclone events which occur within the baroclinic life cycle, in particular, an event which occurs after day 8 and can be seen in the leveling off of global eddy kinetic energy (KE) after day 8.

b. Frontal cyclone development

The low-level temperature and surface pressure at day 6 are shown in Fig. 3. At this stage in the life cycle strong surface frontal zones have formed. The cold front and associated pressure trough are well marked. There is also a strong warm front ahead of the warm sector and strong gradients west of this around the low pressure system forming a bent back baroclinic zone. This type of feature would often be marked as an occlusion on analyzed surface charts but clearly no lifting of warm sector air is necessary to produce the structure seen here. Also of interest is the patch of warm air that has been pinched off into the center of the low. This "seclusion" is the surface analogue of interior PV cut-off events which occur on isentropic surfaces. It is clear that the warm air has been advected into the center of the low and could not have been formed through diabatic processes. The center of a small isolated region of descent is marked on Fig. 3(a). This appears to be

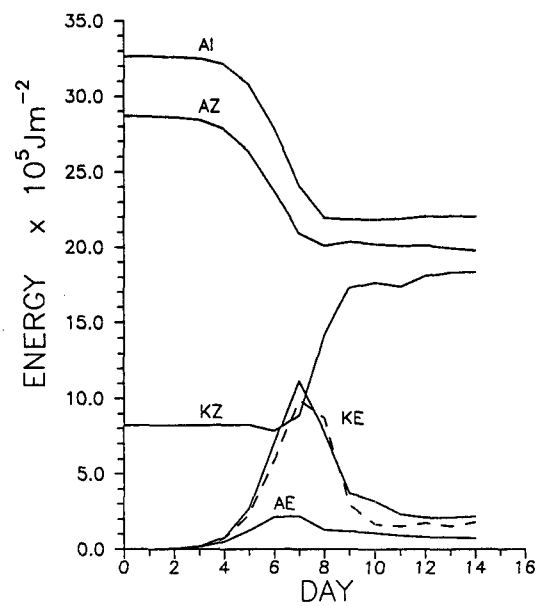

FIG. 2. Evolution of global energy components of the basic life cycle. AI is the "static stability" part of the available potential energy and has had 130×10^5 J m^{-2} subtracted for ease of plotting. AZ is the meridional temperature variance part of the available potential energy, AE is the eddy available potential energy, KE is the eddy kinetic energy and KZ is the zonal kinetic energy. The dashed line is the eddy kinetic energy for the T42 15-level life cycle.

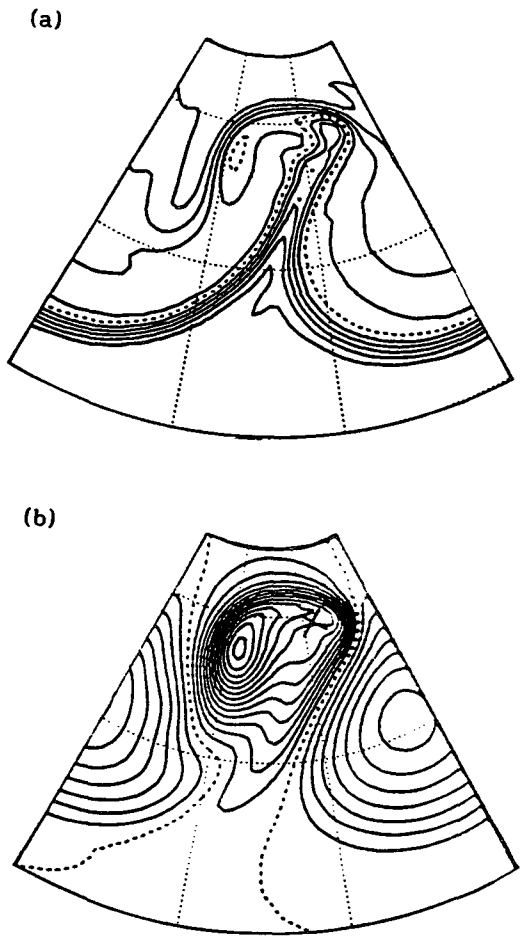

FIG. 3. (a) Temperature at $\sigma = 0.992$ in the basic life cycle at day 6. Contours are drawn every 4 K with the 0°C contour dashed; and (b) surface pressure perturbation at the same time. Contours are drawn every 4 mb with the zero contour dashed. The cross marks the center of a small region of low-level descent. Sectors are shown between 20°N and 70°N. Latitudes and longitudes are dashed every 20°.

important in the formation of small-scale frontal waves to the south west of this and will be discussed below in section 4.

The cold frontal zone has a horizontal surface temperature gradient of about 7°K (100 km)$^{-1}$ at this time. It is also fairly extensive starting from about 50°N to the northeast of the low, stretching southwestward and around the anticyclone. This is the type of front Bjerknes (1919) envisaged to be unstable, and we are therefore interested in the possibility of the formation of cyclones along it.

Figure 4 shows the evolution of the low-level temperature between day 6 and 10. Between day 6 and 7 the region of strong baroclinicity in midlatitudes near 50°N has decayed, resulting in a separation of the frontal zones to the north and south in this occlusion-like process. The separation is more complete by day 8. By day 9 there is an indication of a wave on the old cold frontal zone. By day 10 the front has become further distorted; indicative of a significant frontal cyclone development. Note also that the warm front in this cyclone is stronger than the cold front which has weakened. Hoskins and West (1979) showed that basic flows with significant cyclonic shear produce primary warm fronts and weak cold fronts. Since the frontal cyclone seen here has developed on a cold front characterized by such a shear, it is consistent that a stronger warm front has evolved.

The equivalent wavelength of the frontal cyclone is about 1000 km and the growth rate, although not strictly definable, exceeds 1 day^{-1}. After day 10 the frontal cyclone decays, indicative of the transient nature of the development.

It is of interest to find such a realistic frontal cyclone feature in this idealized study. It suggests that the essence of such frontal cyclone developments can be understood using dry dynamics and that they might be part of the natural evolution of the baroclinic life cycle. Many life cycles occurring in the atmosphere exhibit similar developments late in the time evolution and could be evolving in a similar manner to that seen here. It is also noticeable that only one frontal cyclone is formed and not a family, as suggested by Bjerknes and normal mode theories.

The frontal cyclone development can be understood most clearly by examining the PV evolution. This is achieved here by presenting PV on the 310 K isentropic surface. Initially, the 310 K surface slopes from about 300 mb at the pole to about 700 mb at the equator. Fig. 5 shows the PV evolution from day 6 to 10. Included in these figures are the wind vectors relative to the moving system. On days 6 and 7 the system speed is taken to be that of the normal mode phase speed but at day 8 and after it is taken to be the 6° day^{-1} westward movement of the base of the trough. It is interesting that the high PV on the 310 K surface has wrapped up cyclonically by day 6. This behavior is the same as that of the warm surface temperature [see Fig. 4(a)]. Note that warmth at the surface acts in the same way as high PV in inducing flow anomalies. High PV has moved equatorward into the jet maximum and turned northward again parallel to the surface cold front resulting in a fairly complicated three-dimensional structure. The smaller scale trough structure is obviously not associated with the linear growth of a sinusoidal perturbation of the PV contours. The large scale wave is sinusoidal in structure as indicated by the PV contours and wind vectors. There has also been a tendency for the 0.5 PVU contour to be pulled out around the anticyclone, indicative of the upper-level wave breaking event.

In this life cycle, after the period of cyclonic wrapping up north of the mean jet, there is a transition period when the trough base extends south of the zonally averaged jet. It subsequently tilts in the northeast–southwest direction, consistent with the ambient anticyclonic shear, resulting in poleward momentum fluxes and barotropic decay. This transition occurs between day

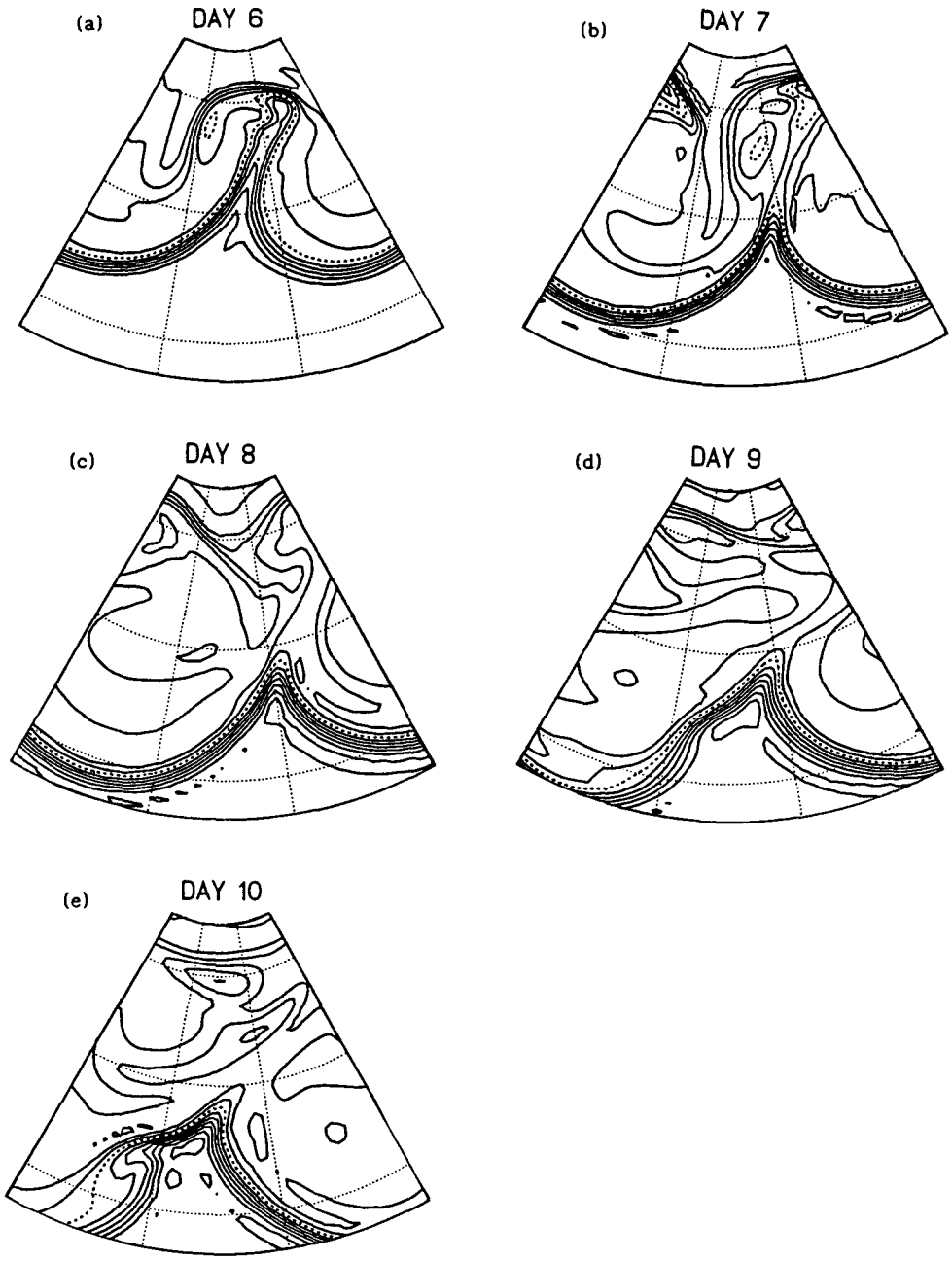

FIG. 4. Temperature at $\sigma = 0.992$ in the basic life cycle between days 6 and 10. Contour intervals are drawn every 4 K with the 0°C contour dashed. Sectors are shown between 15° and 70°N. Latitudes and longitudes are dashed every 20°.

6 and 7. Indeed by day 7 the trough extension and northeast–southwest tilt are evident. The fact that the trough becomes dominated by the anticyclonic shear is crucial to the subsequent trough developments.

As the high PV is wrapped around the anticyclone, the trough thins markedly. This is seen clearly between day 7 and 8. Some appreciation of the mechanism by which this takes place can be gained by examining the wind vectors at this time. On the western side of the trough to the north, strong system relative westerlies exceeding 50 m s^{-1} blow approximately perpendicular to the PV contours while on the leading edge the relative flow is more parallel to them. This implies a convergence of PV contours of the same value and continual thinning. By this stage the 2.0 PVU contour has already closed off.

By day 9 the 1.0 PVU contour has also closed forming a major cut off in PV. The 0.5 PVU contour, however, is still attached to its stratospheric source in the form of a thin "umbilical cord" or shear line. A similar

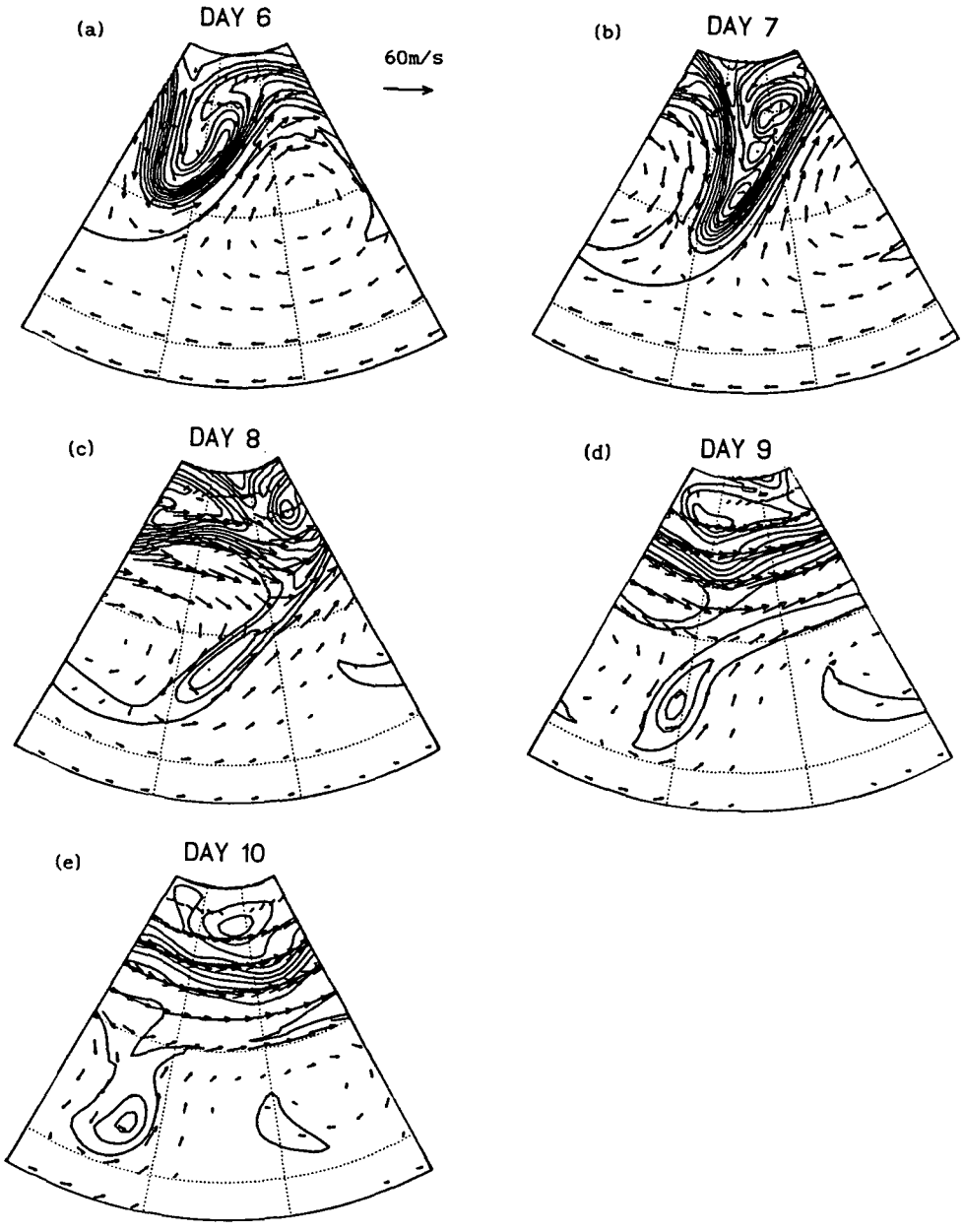

FIG. 5. Potential vorticity on the $\theta = 310$ K surface in the basic life cycle between days 6 and 10. Contours are drawn every 0.5 PVU. System relative wind vectors are included. Up to day 7 the phase speed is taken as that of the normal mode, whereas after this the westward velocity of the trough base is used. The sectors shown are as in Fig. 4.

event has also been seen in a high resolution barotropic integration by Juckes and McIntyre (1987). The final cutting off process, whereby contours from either side of the trough join, must be a dissipative process. Indeed the peak PV value in the trough from day 7 to day 8 has decreased from about 5.5 PVU to about 2 PVU. It is probable that some of this reduction can also be accounted for by advection of the highest valued PV air polewards out of the thinned region.

Comparing the PV cut off location and the position of the frontal cyclone in the low-level temperature field, which was first clearly visible at day 9 (see Fig. 4d), it is highly suggestive that the cyclone has formed because of an interaction between this cut off and the surface frontal zone. The PV cut off has distorted the front creating a positive and negative temperature anomaly. This results in an energetically favorable configuration for baroclinic growth. Barotropic energy conversions will also be important in such a strong frontal zone.

There is a prominent PV anomaly throughout much

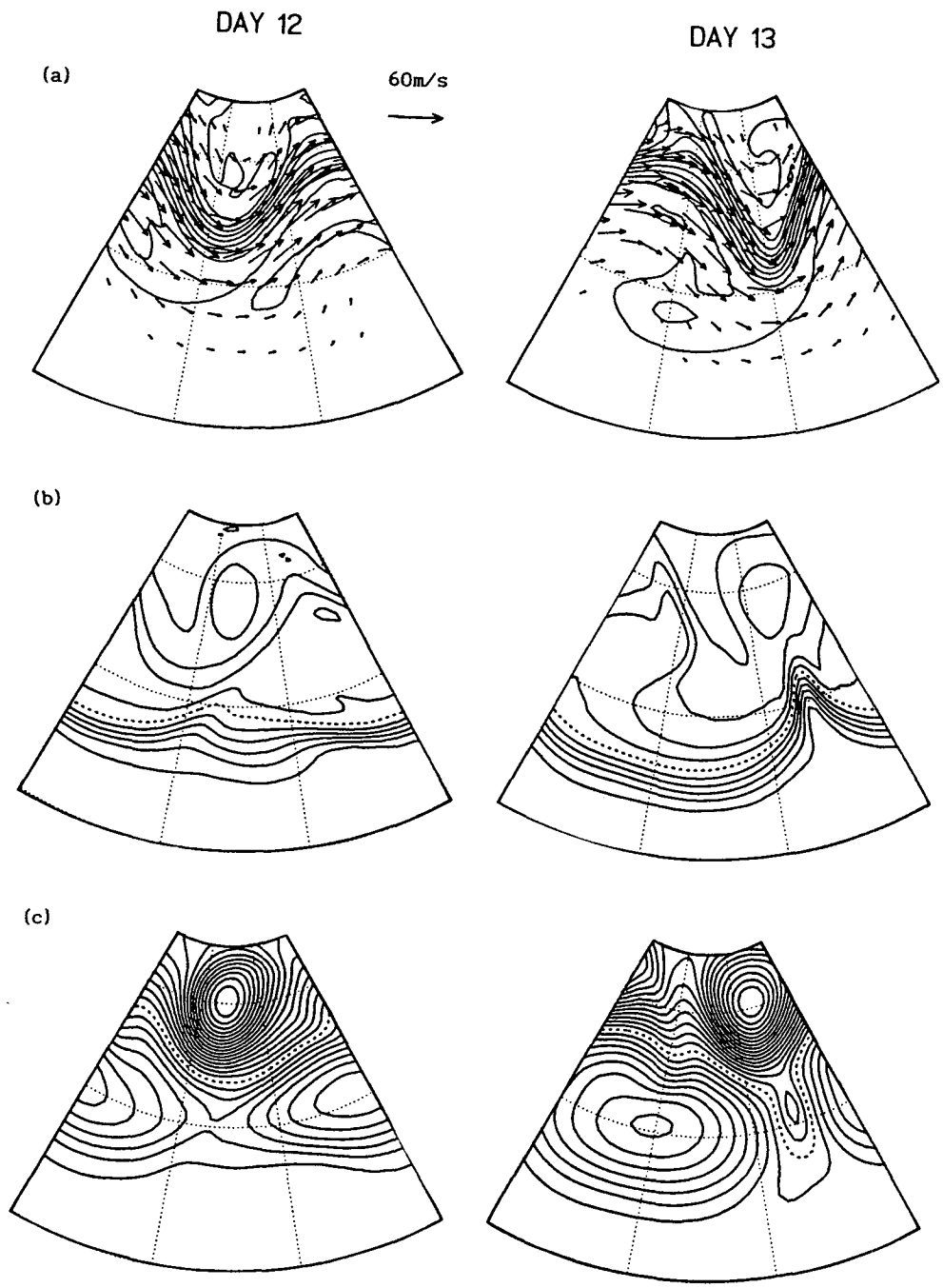

FIG. 6. (a) Potential vorticity on the θ = 310 K surface in the W55 life cycle between days 12 and 13. Actual wind vectors are included. (b) Temperature at σ = 0.967 and (c) surface pressure perturbation at the same time. Contour intervals are as in Fig. 3 and Fig. 5. Sectors are shown between 20° and 70°N. Latitudes and longitudes are dashed every 20°.

of the troposphere. Thus, although the horizontal scale of the frontal cyclone is only about 1000 km, it has considerable depth.

By day 10 the PV cut off on the 310 K surface has evolved into a more circular vortex having become separated from its source region in the polar stratosphere and more influenced by its own cyclonic circulation. The surface cyclone has its largest amplitude at this time. Prolonged normal-mode type growth, resulting from a locking on mechanism, does not occur because the positive PV anomaly cannot be increased by the advections associated with the flow induced by the surface temperature anomaly, a consequence of the closed nature of the PV contours. Indeed, it may

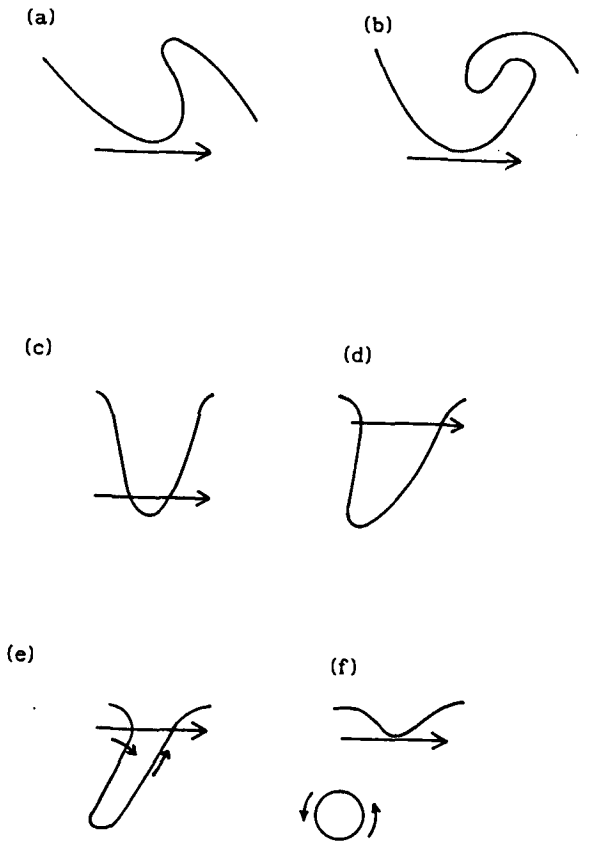

FIG. 7. Schematic evolution of an isentropic potential vorticity contour during the basic life cycle. The thick vector marks the position of the zonal mean jet. Thin vectors mark system relative winds.

be commented here that, since the low-level temperature gradient is in the form of a front, locking-on in these types of situations is never likely to occur for long because cross-frontal displacements have only limited ability to reinforce the low-level temperature perturbation. If the frontal width $l = 100$ km and a cross-front wind $v = 10$ m s^{-1}, the approximate time for the front to be totally distorted is $l/v \approx 10^4$ s. The same argument applies to upper frontal zones or jet streaks.

After day 10, with the lack of phase locking, the structure is sheared apart by the strong vertical shears in the cold frontal zone.

The frontal cyclone development in the model may therefore be viewed as a finite amplitude, transient interaction between an upper tropospheric PV cut-off and a surface front.

c. *A trough tip development*

Another finite amplitude development occurred in a high resolution, T95, 15 level integration of the W55 life cycle of SH. The initial state for this has the same temperature field as the basic case discussed above, but with a 10 m s^{-1} westerly included at 55°N.

The increased cyclonic shear north of the jet, meridionally confines the trough development in the early stages of the life cycle. Later, however, an interesting development is initiated by the PV trough tip. The PV at day 12 and 13 for this life cycle is shown in Fig. 6 along with the low-level temperature and surface pressure fields. The PV shows a sharpening and equatorward movement of the trough between these days. During this time the PV tip interacts with the low-level frontal zone. This is indicated in the temperature field as a wave development in the region of the trough tip. A surface low pressure region also develops during this period. The growth rate for this event is equivalent to about 3 days^{-1}.

d. *Discussion*

The nonlinear frontal cyclogenesis events presented above are simple model developments which have many similarities with those that occur in the real atmosphere. The PV and low-level temperature evolution offer an enlightening view of these nonlinear features.

Finite amplitude frontal cyclone development as described above requires an interior PV anomaly for its initiation. The main reservoir of high PV is in the stratosphere, where midlatitude values exceed 2 PVU. The main way this reaches tropospheric levels, where it can initiate frontal cyclogenesis, is through excursions on sloping isentropic surfaces associated with evolving baroclinic waves. The basic life cycle offers a clear view of how this can occur. The trough evolution for the basic life cycle is shown schematically in Fig. 7. During the linear growth phase of the life cycle the PV trough tilts in the northwest–southeast direction north of the jet maximum. This is in agreement with the conclusions of McIntyre (1970) that unstable baroclinic normal modes growing in a horizontally sheared environment will tend to tilt with the shear. The momentum flux convergence associated with this acts to damp the mode. It will be shown that the basic state horizontal shear is crucial to the surface frontal developments as described by Hoskins and West (1979) and that the original shear and evolving shear also determines the nonlinear trough developments.

After the relatively short period of linear growth (as compared to the duration of the life cycle) the low-level saturation event takes place. At this time the PV trough wraps up cyclonically in a spectacular manner north of the mean jet. This has important implications with regards to likely three-dimensional frontal structure, such as kata and ana fronts. In this instance, the PV is advected parallel and behind the surface cold front and does not overrun as might be expected in a kata front situation. This may be due to the strength of the front and the dominance of the vertical shear in advecting air polewards rather than allowing some form of propagation or drift eastwards over the surface baroclinic zone.

After this, with increasing upper-level wave amplitudes, the base of the PV trough extends through the mean jet to become affected by the anticyclonic shear

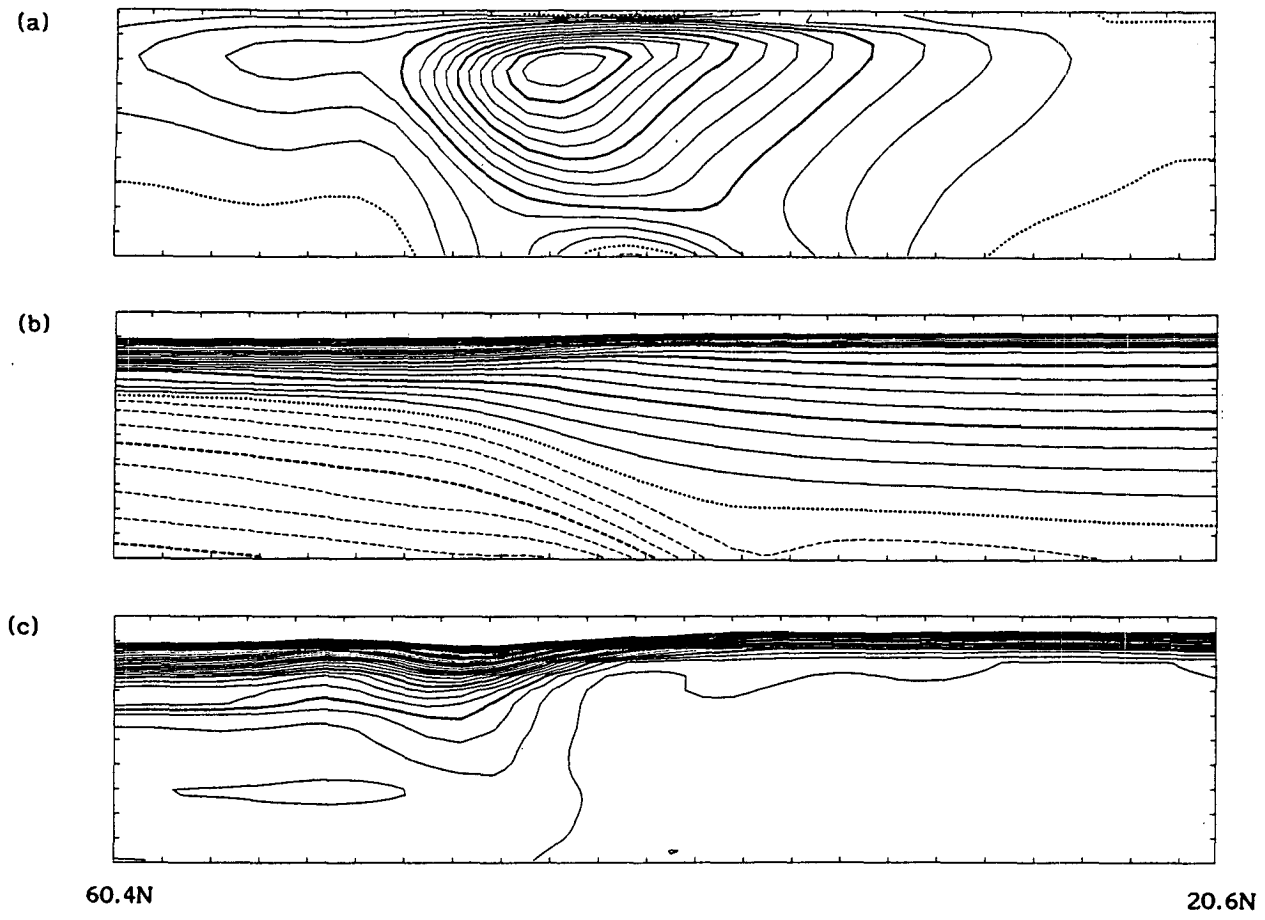

FIG. 8. Basic state used in the frontal stability study. Sections shown between 60.4°N and 20.6°N are: (a) zonal wind, (b) potential temperature, and (c) potential vorticity. Contour intervals are 5 m s^{-1}, 5 K, and 0.5 PVU, respectively. Tick marks on the horizontal axis are every 200 km and on the vertical axis they are every 100 mb with 1000 mb at the ground.

side of the jet. This event is crucial to the subsequent trough development. The increased dominance of this shear causes the trough to become tilted in the northeast–southwest direction and the momentum fluxes are again in the right sense for barotropic decay. The momentum fluxes act in the sense of increasing the shear, and the trough continues to be sheared out. It is clear from the life cycle that the trough does not become stretched in a passive manner. As the trough thins, a PV cut off is eventually formed. As shown in the life cycle, this cut-off can interact with the low-level frontal zone to produce a frontal cyclone. Note also from Fig. 5 and Fig. 7 that once the cut-off has been formed a new trough tip is left to the north. This disrupted trough may also be dynamically active and initiate cyclogensis if it interacts with a surface baroclinic region. This did not occur in the life cycle, but in several real events which we examined the trough to the north of a cut off subsequently moved rapidly eastward steered by the main jet and did in fact initiate significant cyclogenesis. Note that for this poleward feature, reinforcement by meridional advection and phase locking are possible.

The horizontal shear of the basic flow is crucial in determining the likely nonlinear developments. In a life-cycle using the same basic state as shown here but with added cyclonic shear (the EW case of SH) the nonlinear evolution is quite different. The linear phase is similar, and the trough wraps up cyclonically as before but instead of extending through the jet maximum the trough continues to be influenced by the cyclonic shear poleward of the jet. A large scale cyclone persists and decays slowly.

3. Linear study

a. Dry analysis

To contrast with the finite amplitude nonmodal discussion presented above, it is of interest to determine the linear stability of the basic cold front. This has been performed by taking the mass distribution from a section across the cold front at day 6, just north of 40°N in Fig. 3a, rotating this to the meridional direction and using it to construct a balanced zonal flow. This is achieved by demanding that the divergence and divergence tendency are zero using the method described in Hoskins and Simmons (1975).

The resulting basic state is shown in Fig. 8 in terms of u, θ, and PV. It consists of a strong baroclinic zone with a maximum horizontal surface temperature gradient of about 6°K (100 km)$^{-1}$ and an associated jet maximum of 69 m s^{-1} at 44°N. The u section indicates strong vertical and horizontal shears in the frontal zone. The latter shears are strongest on the poleward side where they exceed 10^{-4} s^{-1}. We therefore expect both baroclinic and barotropic energy conversions to be important for modes which grow on this front.

Comparing the PV and θ distributions it is clear that the meridional gradients in PV along isentropes are dominated by the tropopause structure. Together with the meridional surface temperature gradient the necessary conditions for instability are satisfied. There is also a weak surface temperature maximum ahead of the surface front. This is equivalent to a maximum in PV and implies a reversal in gradient thereby satisfying the necessary conditions for instability. This instability has been investigated by Schär and Davies (1989) in a recent semigeostrophic study.

The basic state frontal zone used here is more realistic than in most previous studies, in particular in having tropospheric PV gradients. This enables us to assess more confidently the possible role of modal growth in the frontal cyclone problem.

It should be remembered that the strong cold fronts observed in the atmosphere and indeed in the life cycle do not extend around the globe and are usually less than about 5000 km long. This means that although modes with wavelengths of 3000–5000 km typical of the longer waves will be found, they are not relevant. Our concern here is with wavelengths in the 1000–2000 km range.

The most unstable mode for a particular zonal wavenumber is found using the initial value method adopted by Brown (1969). The T95, 30 level primitive equations are integrated using as initial conditions the zonal flow and a small perturbation confined to the zonal wavenumber of interest. In order to keep the integration linear, the perturbation amplitude was reduced when it became too large. The growth of the perturbation is followed until it is exponential to within a specified accuracy. The growth rate, phase speed, and structure of the most unstable normal mode can then be examined directly. Details of this calculation are given in Simmons and Hoskins (1976). The model was integrated in most cases until the relative change in growth rate between one instant and 0.5 days later was less then 10^{-3}. The calculation is particularly efficient in the vicinity of growth rate maxima but difficulty is found when the second most unstable mode has a growth rate comparable to the most unstable one.

Figure 9 shows the growth rate and phase speed curves for the most unstable modes as a function of zonal wavenumber, m. Two branches are evident from these curves and are identified clearly by the markedly different phase speeds. The first, large-scale Charney-Eady branch has a peak growth rate at $m = 9$ which

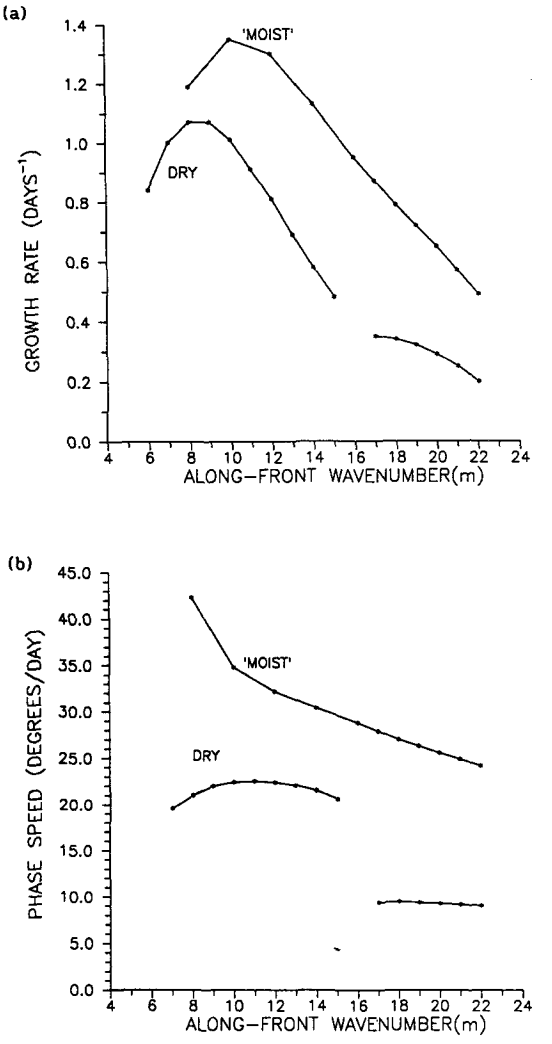

FIG. 9. Growth rate and phase speed curves obtained in the linear analysis of the front shown in Fig. 8. Results for the dry and "moist" analysis are indicated.

corresponds to a zonal wavelength of about 3400 km. The phase speeds for these modes are around 20° day^{-1} implying a steering level at about 800 mb. The most unstable mode for $m = 16$ could not be found. As can be seen from Fig. 9, this wavenumber is in the region where the two branches cross, and as already remarked above, it is always difficult to find the most unstable mode in such cases. The second branch has a plateau around $m = 18$, which corresponds to a wavelength of about 1600 km. The phase speed for these modes is about 10° day^{-1}, implying a steering level much closer to the ground. Since this branch is in the 1000–2000 km range this mode may be of some interest for the frontal cyclone problem. However, its growth rate is only 0.34 days^{-1}. Thus, despite the strength of the front, the frontal cyclone scale mode has a relatively small growth rate. This growth rate should be compared with the equivalent finite amplitude growth in the basic life cycle, which exceeds 1 day^{-1}.

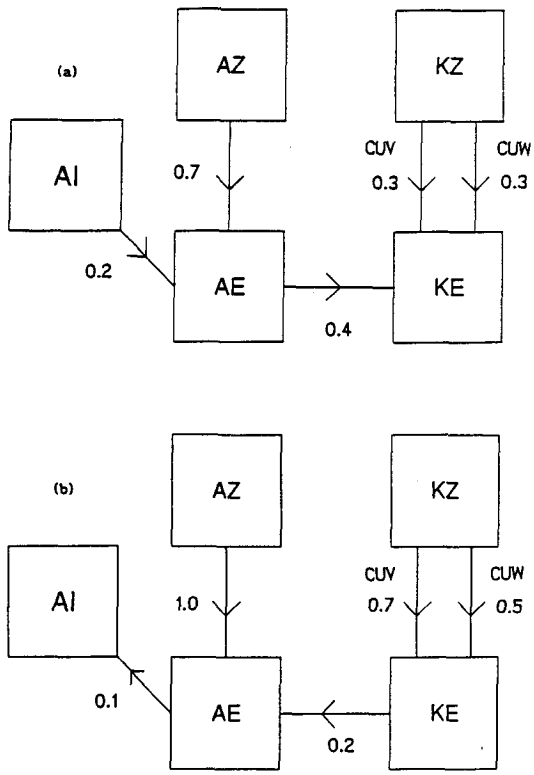

FIG. 10. Energy box diagrams indicating the energy conversions of the most unstable (a) $m = 10$ mode and (b) $m = 18$ mode. For classification of the energy variables see Fig. 2. and Pearce (1978). CUV and CUW represent the horizontal and vertical Reynolds stress terms, respectively.

The energy box diagrams for the most unstable $m = 10$ and $m = 18$ mode are shown in Fig. 10. The conversions are normalized so as to give a net conversion to KE of 1. The conversion between KZ and KE has been split between the horizontal and vertical Reynold's stress terms CUV and CUW, respectively. The modes on the first, lower wavenumber branch, as typified by the $m = 10$ mode, gain significant energy from both the potential and kinetic energy of the basic flow and represent a modified Charney-Eady type mode.

The $m = 18$ mode however is not characterized by baroclinic energy conversions. Instead, it converts KE into AE. The KE grows at the expense of both horizontal and vertical wind shears in the frontal zone. This resembles the energetics of the weakly growing mode found by Schär and Davies (1989).

The $m = 18$ mode is confined to very low levels and is apparently not influenced by the tropopause. It is only the strong wind shears in the surface frontal zone that are important.

The zonal mean KE for this mode shown in Fig. 11 indicates its shallow nature, with its amplitude decreasing to less than 10% of the surface maximum by $\sigma = 0.9$. The maximum is located on the cold side of the main temperature contrast in the region of anticyclonic shear. The horizontal heat flux, although positive, is also confined to below $\sigma = 0.9$. The vertical heat flux has positive and negative values, with the global average of the corresponding energy conversion term being slightly negative as seen in Fig. 10.

The zonal mean horizontal and vertical momentum fluxes also indicate the shallowness of the mode. The horizontal momentum fluxes are largest and negative on the cold anticyclonic side of the front at the surface consistent with a positive conversion KZ $\Rightarrow$ KE. The vertical momentum flux is positive resulting in a positive baroclinic shear conversion.

b. *"Moist" analysis*

The possible role of latent heat release in the linear frontal cyclone problem is examined here by repeating the above analysis with the very simple parameterization used by Bennets and Hoskins (1979). An extra diabatic term proportional to $-\omega$ is included in the thermodynamic equation when there is ascent. As in

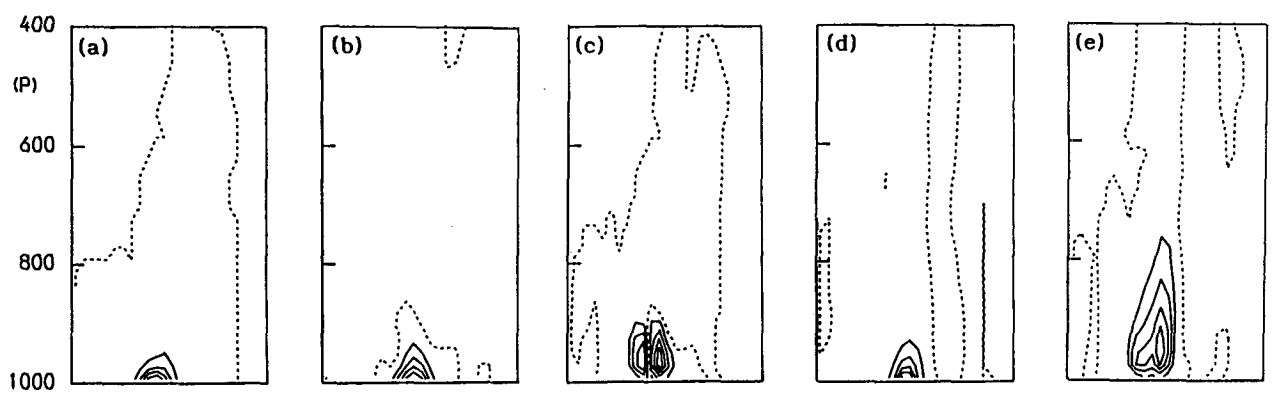

FIG. 11. Latitude–height sections of zonal mean (a) eddy kinetic energy, (b) horizontal heat flux, (c) vertical heat flux, (d) horizontal momentum flux and (e) vertical momentum flux for the most unstable $m = 18$ mode. Each variable is plotted with a contour interval 0.2 times the extreme value. Sections are shown between 30°N on the left and 60°N on the right. Extrema for each flux when the fields have been scaled to give a surface pressure perturbation of 3 mb are (a) $[v^{*2}] = 147\ \text{m}^2\ \text{s}^{-2}$, (b) $[v^*T^*] = 31\ \text{m s}^{-1}$ (°C), (c) $[\omega^*T^*] = -7$ mb h^{-1} (°C) (poleward extremum), (d) $[u^*v^*] = -77\ \text{m}^2\ \text{s}^{-2}$ and (e) $[v^*\omega^*] = 13\ \text{m s}^{-1}$ mb h^{-1}.

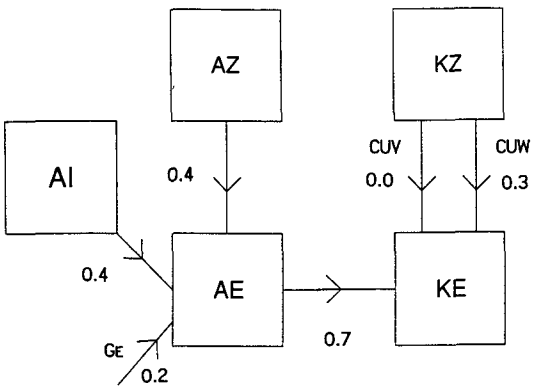

FIG. 12. Energy box diagram indicating the energy conversions of the most unstable moist $m = 18$ mode. For classification of the energy variables see Fig. 2. and Pearce (1978). CUV and CUW represent the horizontal and vertical Reynolds stress terms, respectively. The quantity G_E is the generation term due to the latent heating.

Bennets and Hoskins (1979), the extra heating obtained during ascent is approximately equivalent to rising up a $\theta_w = 10°C$ moist adiabat. This parameterization assumes that the air is saturated everywhere and no account is taken of the variations of saturation with temperature or of evaporational cooling. Further, no account is taken of convective rainfall. However, several studies (e.g., Reed et al. 1988) have shown that the heating in cyclones attributed to convection to be only about 10% or less. We may therefore feel confident that we are including the major diabatic term in the thermodynamic equation. It should be noted that the effect of latent heat release has only been included after 6 days of dry frontogenesis. The changes to the frontal structure resulting from moist frontogenesis have not been considered.

The growth rate and phase speed curves as a function of zonal wavenumber m with this latent heat parameterization are included in Fig. 9. Growth rates increase for all wavelengths but more so for smaller scales indicating an increased sensitivity at these scales. The curves for the most unstable modes show only one modal branch, the shorter waves forming the tail of the Charney-Eady type branch. The growth rate for the $m = 18$ mode has more than doubled to 0.79 days^{-1}. The phase speed for all modes has increased and that for the $m = 18$ mode has increased to 27 m s^{-1} indicating a much higher steering level than before (just below 700 mb). The global energetics for the moist $m = 18$ mode is shown in Fig. 12. The energy box diagram now includes an extra term G_E, for the generation of eddy available potential energy by the latent heating. The energetics have changed markedly with the inclusion of latent heat release and are now dominated by baroclinic conversions, with a large direct conversion from AE to KE. The shear conversion term is dominated by the CUW term consistent with a reduced effective N and increased vertical velocity. The direct moist effect, as measured by G_E is less important than the indirect effect due to change in structure.

The zonal mean EKE for the $m = 18$ mode shown in Fig. 13a indicates the increased depth of the mode relative to the dry case reaching less than 10% of its surface maximum value only by $\sigma = 0.67$. It is also apparent that the mode is now concentrated more on the warm side of the cold front. The horizontal and vertical heat fluxes (Figs. 13b,c) confirm the increased importance of baroclinic conversions.

The vertical momentum flux (Fig. 13e) is similar to that of the dry mode but deeper. The horizontal momentum flux (Fig. 13d) has both signs in the region of the westerly maximum ahead of the surface front resulting in the small residual CUV conversion in Fig. 12.

Figure 14 shows the vertical structure of the mode normalized to give a surface pressure perturbation of 3 mb and added to the basic state. These sections are through the latitude of maximum meridional wind at 39.2°N. There is a reduction in the horizontal scale of the ascending air, which is in agreement with the work

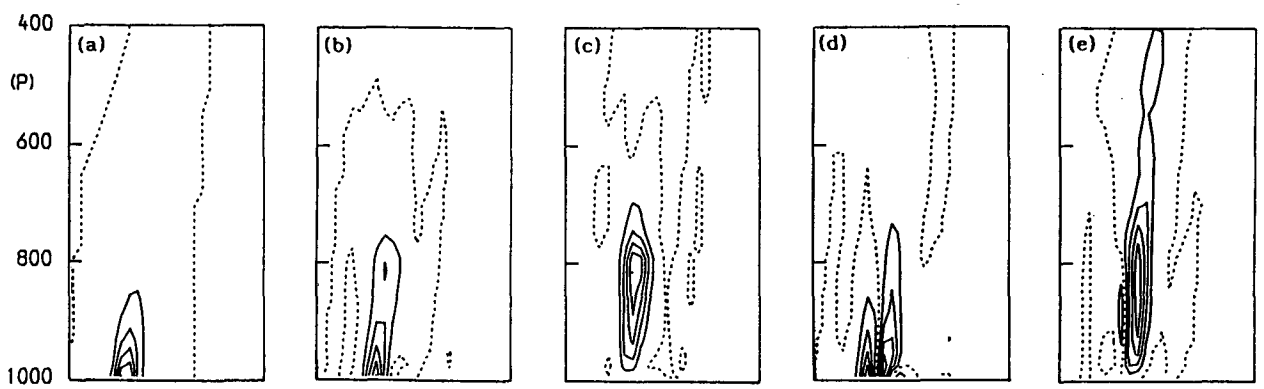

FIG. 13. Latitude–height sections of zonal mean (a) eddy kinetic energy, (b) horizontal heat flux, (c) vertical heat flux, (d) horizontal momentum flux and (e) vertical momentum flux for the most unstable "moist" $m = 18$ mode. Each variable is plotted with a contour interval 0.2 times the extreme value. Sections are shown between 30°N on the left and 60°N on the right. Extrema for each flux when the fields have been scaled to give a surface pressure perturbation of 3 mb are: (a) $[v^{*2}] = 56$ m^2 s^{-2}, (b) $[v^*T^*] = 7$ m s^{-1} (°C), (c) $[\omega^*T^*] = -8$ mb h^{-1} (°C), (d) $[u^*v^*] = 9$ m^2 s^{-2} (equatorward extremum) and (e) $[v^*\omega^*] = 8$ m s^{-1} mb h^{-1}.

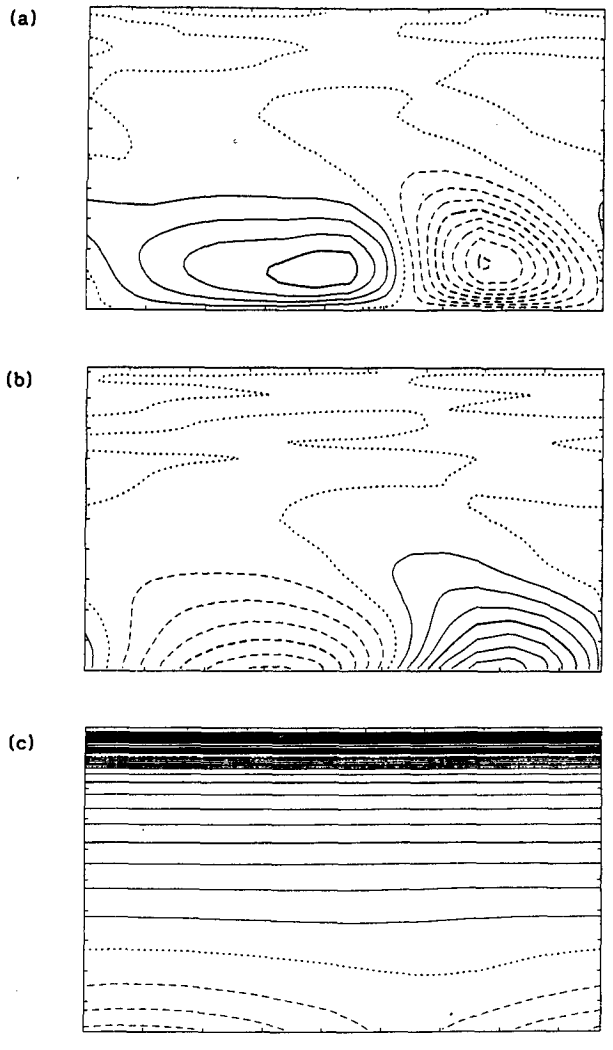

FIG. 14. Vertical sections at the latitude of maximum meridional wind for the most unstable "moist" $m = 18$ mode. The mode has been normalized to give a minimum surface pressure perturbation of 3 mb. Sections are shown for: (a) vertical velocity, (b) meridional wind, and (c) potential temperature. Contour intervals are 0.15 mb h^{-1}, 1 m s^{-1} and 5 K, respectively. Tick marks on the horizontal axis are every 200 km and on the vertical axis they are every 100 mb with 1000 mb at the bottom.

of Emanuel et al. (1987). The ratio of ascent and descent widths is 0.62 resulting in an ascent width of about (660 km). The ascent maximum is about 1.8 times the descent maximum value. Strongest horizontal gradients in ω occur on the western edge of the ascent in agreement with the moist structures found by Emanuel et al. (1987). Asymmetry is also evident in the meridional wind with stronger narrower southerlies in the warm air and weaker broader northerlies in the cold air.

c. Frontal wave forcing in the life cycle

As discussed above, the present normal mode calculations make the traditional assumption that the basic state is steady. In order to see if an evolving front can support growing small scale waves, the front at day 6, which has been shown to be linearly unstable, has been given a 1500 km wavelength perturbation. This perturbation was produced by a forcing that took the form of a transient heating and cooling along the front. The forcing is not meant to represent any atmospheric process but is simply a means of perturbing the front with a frontal cyclone scale wavelength. The results presented here have used a vertical heating profile that reduces from a maximum at the surface to zero at $\sigma = 0.5$ and above. The solutions have been found to be insensitive to this profile. The heating and cooling was switched on at day 6, moved eastward with the front and switched off at day 6.5. The integration was then continued to see if any growth occurred.

Some day 6.5 fields for a 40 K day^{-1} maximum heating rate are shown in Fig. 15. A 1500 km wave is clearly evident together with the associated relative vorticity maxima and minima. The low-level temperature and vorticity fields half a day later are also shown in Fig. 15. Virtually all trace of the temperature wave has disappeared and the anomalies in the vorticity field have been sheared out. Further integration has shown the basic life cycle to be almost unaffected by the forcing. Thus, despite the instability of the steady front, the perturbation rapidly decays implying that the evolving front is in fact stable.

It is clear that the reason for this difference is the invalidity of the two-dimensional steady assumption made in the linear instability problem. As shown by the **Q** vectors at day 6 in Fig. 16. There is still active frontogenesis, with the arrows pointing towards warm air. A typical magnitude of **Q** in the cold front region at day 6 is about $12°K\,(100\,km)^{-1}\,day^{-1}$. This implies a frontal forcing time scale of $\approx$½ day, which is significantly shorter than the time scale for dry normal mode growth obtained in the linear stability study seen above. Thus, although a two-dimensional steady version of this front is linearly unstable, the deformation present in the evolving front suppresses it.

It should be noted, however, that Joly and Thorpe (1990c) have shown that, in a case where the front is forced by horizontal shear, linearly unstable modes may still exist.

4. Upstream development mechanism for frontal cyclogenesis

It has already been noted in the life cycle that during the cyclonic wrap up of low-level isotherms, a small isolated region of descent appeared (see Fig. 3b). The surface pressure showed signs of ridging in this region. From it a weak wave-like feature appears in the temperature field (see Fig. 3a) towards the south west along the cold frontal zone. This wave is seen in other fields as well and the feature has also been seen in other life cycles. It is, perhaps, best seen in the life cycle with added barotropic cyclonic shear (the anomalous EW

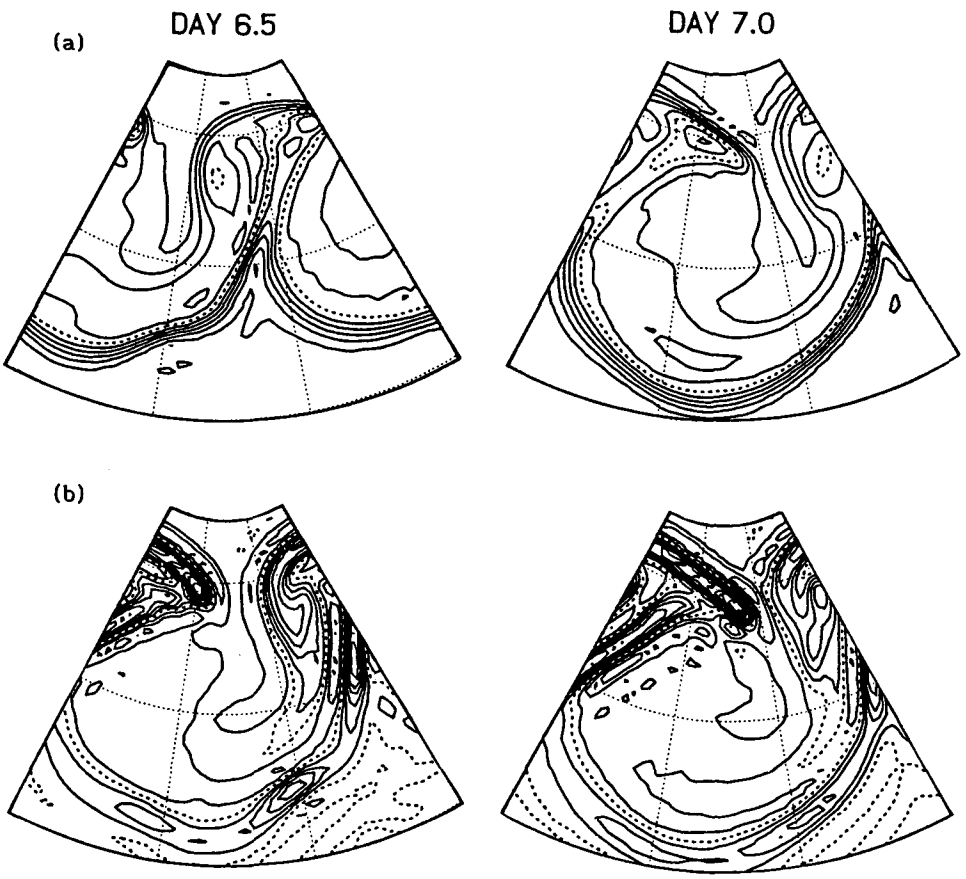

FIG. 15. (a) Temperature and (b) relative vorticity at $\sigma = 0.992$ at day 6.5 after 0.5 days forcing and day 7. Contour intervals are 4 K and 0.6Ω, respectively. Sections are shown between 20°N and 70°N. Latitudes and longitudes are dashed every 20°.

case of SH). In this case, a more intense warm frontal structure is formed and again, as shown in Fig. 17, warm air is secluded in the center of the low and an isolated region of descent is produced. There is a slight indication of a wave in the broad baroclinic region in the cold front zone (see Fig. 17a). This waviness is more marked in the low-level vertical velocity field (Fig. 17c). Development of this wave is seen clearly in cross sections taken parallel to the cold front (see Fig. 18). The sections indicate the evolution of vertical velocity ω along the cold frontal zone between days 4 and 6. The sections are dominated by the large scale ascent in the warm sector and frontal region on the right. However, the growth of the wave pattern identified above is also seen. Between days 4 and 5 a small region of enhanced descent develops at low levels. The descent is only about 1.5 mb h^{-1} and the vorticity in this region about -0.4Ω (where Ω is the earth's angular velocity). Between days 5 and 6 the descent region has continued to increase and further negative ξ is produced. Further south-west along the front, an ascent region has also evolved during this time. The day 6 maximum descent and ascent in the wave are +4.5 and −1.5 mb h^{-1} and the vorticity corresponding to this is -1.2Ω and 0.1Ω. The along front wavelength indicated by this pattern is about 700 km and the disturbance is shallow, decreasing to negligible amplitude above 850 mb. These features are also evident in the same fields in the basic life cycle. Examination of analysed surface pressure fields from the United Kingdom Meteorological Office

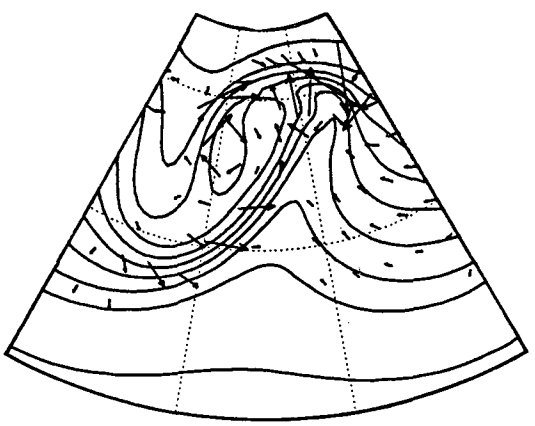

FIG. 16. Potential temperature with Q-vectors at $\sigma = 0.792$ at day 6 in the basic life cycle. Potential temperature contours are drawn every 4 K. The section is shown between 20°N and 70°N. Latitudes and longitudes are dashed every 20°.

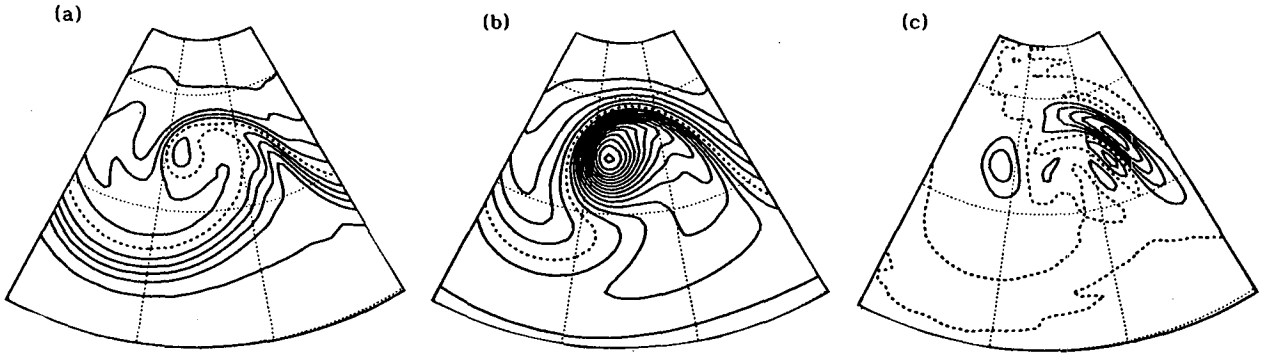

FIG. 17. Horizontal sections at day 6 in the EW life cycle. Sections shown are: (a) temperature at $\sigma = 0.967$, (b) surface pressure perturbation, and (c) vertical velocity at $\sigma = 0.967$. Contour intervals are 4 K, 4 mb, and 0.15 mb h^{-1}, respectively. Sectors are shown between 20°N and 70°N. Latitudes and longitudes are dashed every 20°.

fine mesh model has also shown short cold frontal waves, near the warm front to be a relatively common feature in growing baroclinic waves.

Comparing the 700 km wavelength seen here with the unstable waves found in the linear study above, it is clear that this scale of disturbance is linearly stable. It is suggested that the wave developments seen in the model are the result of an upstream development mechanism. Such a mechanism was originally postulated by Simmons and Hoskins (1979) to be important for cold frontal wave events and the formation of cyclone families. These ideas have recently been extended by Hoskins (1990).

For the two-dimensional Eady model without a lid, only neutral surface trapped normal modes exist. If we take the initial forcing in this case to be a dipole PV disturbance included at a particular level, a train of waves develops. This train is stationary with respect to the PV disturbance and its wavelength is that of the neutral mode whose phase speed is zero in that frame. The packet of waves develops upstream with the neutral mode group velocity, which is the speed of the surface flow. Figure 19 shows longitude–height sections of the streamfunction at the initial instant and at intervals of 3.1 h using typical parameters. For these parameters the wavelength produced is 890 km. It is of interest to note the westward tilt with height of the growing systems and their transient similarity to growing normal modes, even though such modes do not exist. Also, the waves have a very large amplitude compared with that associated directly with the PV perturbation. Details of the analysis of this problem are given in the Appendix.

In the life-cycle the waves are forced during the cyclonic wrap-up of low-level isotherms. A qualitative view of this development of a train of neutral Rossby waves on the surface baroclinicity is illustrated in Fig. 20. A cold frontal zone is indicated oriented in the northeast–southwest direction. The low-level saturation and wrap up of surface isotherms results in a warm surface temperature anomaly to the northeast at the end of the cold frontal zone. This warm anomaly has a cyclonic circulation associated with it. As indicated, the northwesterly winds produced by this warm anomaly extend into the region of the unperturbed surface front upstream, forcing a cold anticyclonic anomaly there. This anomaly reinforces the northeasterly and also its associated southwesterly warm cyclone. In this manner, a series of waves can be produced. If the initial

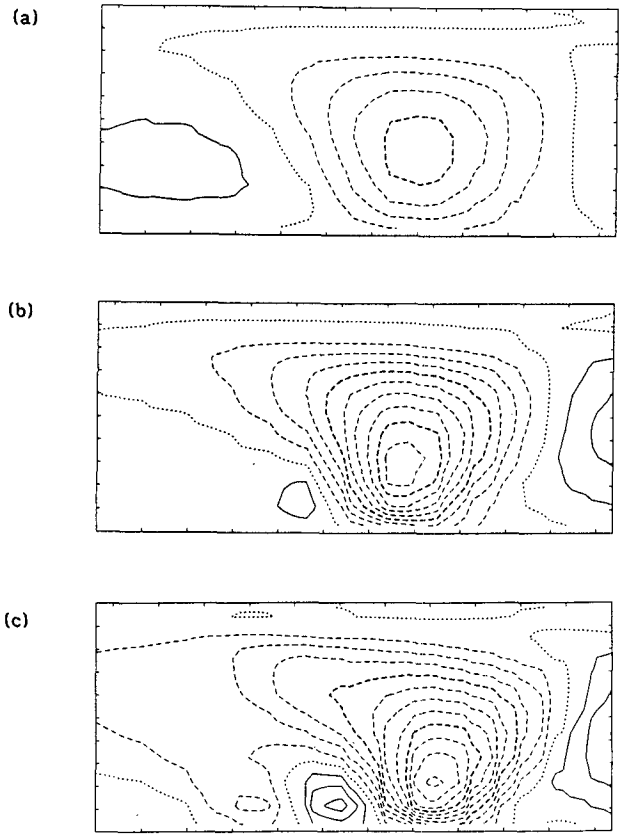

FIG. 18. Vertical sections parallel to the cold front in the EW life cycle showing vertical velocity from 4 to 6 days. The contour interval is 1.5 mb h^{-1}. Tick marks on the horizontal axis are every 200 km and on the vertical axis they are every 100 mb with 1000 mb at the bottom.

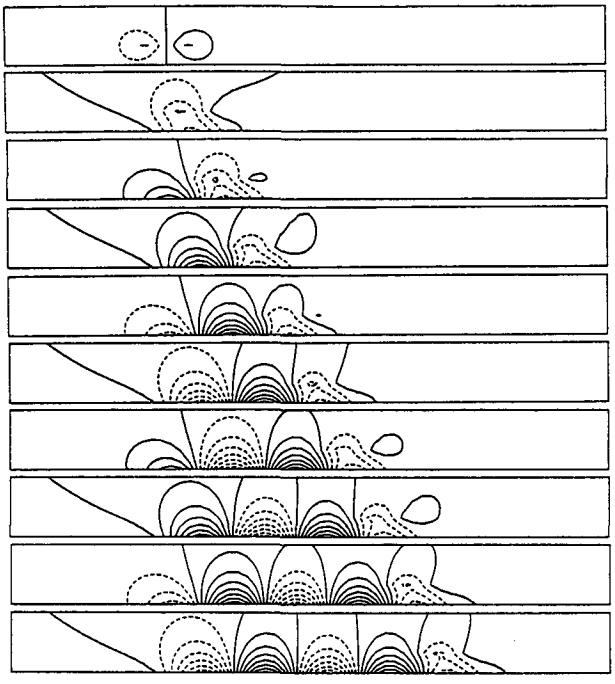

FIG. 19. The upstream development of waves in the two-dimensional neutral Eady model with no lid. The streamfunction is shown in an x–z section for the initial state, corresponding to a PV δ-function in z, and at equal time intervals thereafter. Further details are given in the Appendix. For the parameter values given there, the domain size shown is 8500 km by 3 km, the resonant neutral mode wavelength is 890 km and the time between frames is 3.1 h.

positive anomaly continues to be forced or grows by some mechanism, large growth can result upstream despite these upstream waves being linearly stable. It should be noted, however, that these waves form in a region where the frontal forcing is weak. As in the linear study, one would expect strong deformation to suppress upstream development.

The wavelength observed in the upstream development appears to vary linearly with horizontal resolution. With a T42, T95 and T119 spectral representation the wavelength of the upstream disturbances is approximately 1800 km, 700 km, and 550 km, respectively. Since the wave development is intimately related to the low-level saturation event and the associated cascade towards smaller scales, the decreased wavelength with increased resolution is therefore consistent with an improved representation of this. This indicates that although the model is producing an interesting synoptic event, with possible direct relevance to important developments in the atmosphere, it is dependent on the small scales present in the frontal and occluding regions. The relevant scale in the atmosphere in this occlusion region and the scale of the upstream growth requires further investigation.

The upstream development mechanism might be expected to be stronger in the presence of latent heat release. Indeed, although the wave developments in the dry case above are relatively weak, especially in the temperature wave, when the moist parameterization used in the linear study was included, a more vigorous deeper upstream cyclone evolved. The first cyclone (i.e., vorticity maximum) also forms a few days earlier and has an ascent maximum now exceeding -14 mb h^{-1}.

5. Discussion

This paper has examined possible mechanisms for the initiation of frontal cyclones. In contrast to previous work on frontal cyclogenesis, the present investigation has emphasized finite amplitude initiation, rather than a modal viewpoint, and a description in terms of the PV concepts discussed in Hoskins et al. (1985) has been given. In this view, cyclones result from an interaction between a positive tropospheric PV anomaly and the surface frontal zone.

The main reservoir of high PV is in the stratosphere where midlatitude values exceed about 2 PVU and the primary way in which this reaches tropospheric levels, where it can initiate frontal cyclogenesis, is through the meridional excursions on sloping isentropic surfaces associated with growing baroclinic waves. With this in mind, several baroclinic life cycles have been studied using an idealized spectral model with no diabatic or frictional processes except internal diffusion. PV anomalies associated with latent heat release are therefore not included.

In the basic life cycle discussed in section 2, it was shown how a PV cut off formed from the larger scale trough. This interacted with the surface frontal zone and formed a frontal cyclone which grew with an equivalent e-folding time of less than a day. This trough development is strongly determined by the anticyclonic shear south of the main westerly jet. All troughs seen in the life cycle experiments that have become affected by the anticyclonic shear have formed cut offs in PV. From examination of isentropic PV analyses of European Centre for Medium Range Forecasting data these cut off events are also a common feature in the atmosphere.

Trough developments which are dominated more by the cyclonic shear north of the jet are likely to evolve

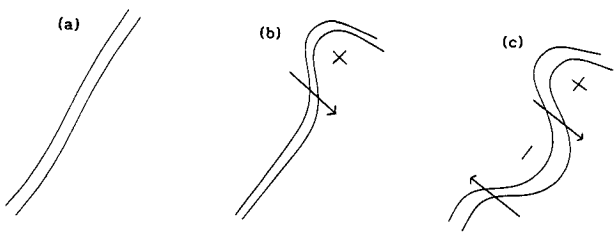

FIG. 20. Schematic of upstream development along a cold front. (a) shows two isotherms in the initial cold frontal region. (b) shows the cold front with a warm anomaly towards the northeast that forms during the cyclonic wrap up of isotherms at low levels. As indicated in (c), the cyclonic vorticity associated with this warm anomaly induces a disturbance upstream.

differently from those on the anticyclonic side. Indeed, the life cycle, with added cyclonic shear (the EW case of SH), is found to be dominated by the cyclonic side of the jet resulting in a large scale cyclonic wrap up and no small scale cut off or frontal cyclone development. It is therefore important to note the apparent "competition" between the northern and southern side of the main zonal jet in determining the nonlinear evolution of PV troughs in the atmosphere.

From the life cycle experiments it has been shown that frontal cyclones can form from the PV provided by the large scale trough, either in the form of a PV cut off or the trough tip. Developments are more likely to achieve really large amplitude if the anomaly is still attached to its stratospheric source and does not cut off. This is because a locking-on and reinforcement mechanism is more likely to occur.

As well as originating from the large scale trough, a positive PV anomaly may also be advected into the trough system from another synoptic event upstream. This anomaly is sometimes referred to as a jet-streak or short-wave trough by synopticians. It can interact with the trough to enhance the cut off process if it arrives late in the life cycle of the large scale cyclone. Alternatively, if it arrives earlier in the life cycle it can be advected into the base of the trough where it may invigorate or initiate low-level cyclonic development.

Synoptic experience has led to the definition of several types of frontal cyclone (see Sawyer 1950). These include warm-front cyclones, triple-point secondaries, which are cyclonic developments in the region where the cold and warm front meet, and cold-front cyclones. Cyclogenesis, resulting from PV interactions with surface baroclinicity, may be viewed differently depending on the relative position of the PV anomalies and surface fronts. For example, in the development shown in section 2.2 the PV anomaly interacts with the cold front in the temperature wave. If, however, the anomaly was only about 8° to the east it would have interacted with the surface baroclinicity where the cold and warm front meet, thus taking on the appearance of a triple-point secondary. The development discussed in section 2.3 shows a PV anomaly interacting with the surface baroclinicity at a crest in the temperature wave and takes on features similar to a triple-point development. Further work is necessary to determine if the different types of frontal cyclone referred to above are dynamically significant or whether, as suggested here, they result from the same PV interaction but at different points in the surface temperature wave.

The stability of the cold front which formed in the basic life cycle has also been studied using a standard normal mode analysis. However, it was shown that the front in the growing baroclinic wave was rendered stable to the growth of small amplitude perturbations by the deformation which was forming the front. This suggests that any linear frontal instability analysis is only likely to be relevant to fronts in mature systems or to a more steady front such as the "Baiu front" in Eastern Asia (see Matsumoto et al. 1970). The linear analysis of a steady version of the cold front, identified only weakly growing surface modes in the 1000–2000 km wavelength range. These were strongly influenced by the horizontal and vertical shears in the surface frontal zone. The small growth rates and shallow nature of these modes suggest that only weak deformation or surface drag will be necessary to suppress them (see Farrell 1985; Valdes and Hoskins 1988). Similar conclusions are relevant to all weakly growing shallow modes found in other frontal cyclone studies.

The linear study was repeated with a simple latent heating parameterization. Even with a relatively weak amount of heating, the Charney-Eady type baroclinic modes were substantially destabilized at the frontal cyclone scale and dominated the "moist" instability analysis. The baroclinic growth rates were increased by a factor greater than 5 with the $\theta_w = 10°C$ parameterization, but are still weaker than the dry finite amplitude growth seen in the life cycles. These moist modes are characterized by a scale contraction in the ascending part of the wave and may have particular relevance to the frontal cyclones sometimes seen on the Baiu front with its weaker deformation and increased importance of moist processes.

Another frontal cyclone initiation mechanism, not depending on the existence of unstable modes, was also suggested by the life cycles examined. This is an upstream development mechanism, originally proposed by Simmons and Hoskins (1979), in which cyclones develop upstream from an initial disturbance on the cold front in the manner of a train of neutral Rossby waves on the surface baroclinicity. The initial disturbance in the life cycle forms during the wrap up of isotherms in the low-level saturation event. Such frontal cyclone disturbances near the warm front appear to be ubiquitous, if rather weak features on analyzed surface charts.

It should be stressed that the above cited mechanisms for frontal cyclone initiation are not necessarily mutually exclusive. Indeed, it is in situations when more than one exist that explosive events are more likely to occur. For example, the October 1987 storm (see Hoskins and Berrisford 1988) appears to result from a combination of shallow surface waves and the interaction of one of these with an upper PV anomaly in a very moist atmosphere. Reed (personal communication) has noticed several vigorous frontal cyclones to result from such a combination of events. It does appear, however, that significant frontal cyclone events in the atmosphere will mostly be associated with finite amplitude growth as discussed above rather than with a linear mode.

With the increased resolution used in this study, synoptic developments have come more into focus and since some were not seen at all at T42 it may be tempting to continue increasing the resolution. At the present time, our understanding of the diabatic processes in the atmosphere requires more immediate research. It is clear that although the initiation of many frontal cyclones events in the atmosphere can be understood

in terms of the dry dynamics, diabatic processes will play an important role. Further work is necessary to understand processes such as: latent heat release, evaporative cooling, surface heat fluxes, friction, conditional symmetric instability and convective instability as they effect the frontal cyclone scale. The material generation and destruction of PV and the advection of such anomalies within the cyclone also requires further investigation. The continued use of simple models is necessary to examine these processes in an idealized context, with the aim of comparing the results with more complicated numerical weather prediction models and available observations.

Acknowledgments. One of us (C.T.) wishes to thank the Natural Environmental Research Council for funding during the time this work was carried out. We also wish to acknowledge Mr. K. Dunn and Mr. K. Spiers for help with some of the figures. We would also like to thank Huw Davies for helpful comments in the review stage of this paper.

APPENDIX

The Excitation of Neutral Two-Dimensional Eady Waves

Consider the Eady problem:

$$\bar{u} = \Lambda z \quad f = f_0, \quad \rho = \text{const.}, \quad N^2 = \text{const.}, \quad \text{(A1)}$$

for a semi-infinite domain $z \geq 0$. Nondimensionalizing variables:

$$\tilde{z} = z/H, \quad \tilde{x} = fx/NH, \quad \tilde{t} = f\Lambda t/N,$$
$$\tilde{\psi} = \psi/A, \quad \tilde{q} = qf^2L^2/(N^2H^2A), \quad \text{(A2)}$$

and dropping the tildes, the quasi-geostrophic equations for y-independent flows may be written:

$$\left(\frac{\partial}{\partial t} + z\frac{\partial}{\partial x}\right)q = 0, \quad \text{where} \quad q = \frac{\partial^2\psi}{\partial x^2} + \frac{\partial^2\psi}{\partial z^2}, \quad \text{(A3)}$$

with

$$\frac{\partial}{\partial t}\frac{\partial\psi}{\partial z} - \frac{\partial\psi}{\partial x} = 0 \quad \text{on} \quad z = 0. \quad \text{(A4)}$$

Substitution in these equations shows that zero PV neutral modes of the form:

$$\psi \propto e^{-kz}e^{ik(x-ct)}, \quad \text{(A5)}$$

are solutions provided that the phase speed $C = k^{-1}$. These neutral modes have a group velocity:

$$c_g = \frac{\partial kc}{\partial k} = 0. \quad \text{(A6)}$$

They are nondispersive with their wave activity propagating at the speed of the surface flow.

Now consider an initial PV distribution which is a δ-function in z and sinusoidal in x:

$$q(x, z, 0) = q_1\delta(z - h)e^{ikx}. \quad \text{(A7)}$$

From (A3) the PV distribution at any time is just:

$$q(x, z, t) = q_1\delta(z - h)e^{ik(x-ht)}. \quad \text{(A8)}$$

The ψ distribution which corresponds to this is

$$\psi = \psi_1 e^{k(z-h)}e^{ik(x-ht)} \quad z < h$$
$$\psi = \psi_1 e^{-k(z-h)}e^{ik(x-ht)} \quad z > h \quad \text{(A9)}$$

where

$$q_1 = \int_{z=h^-}^{z=h^+} q\,dz = \left[\frac{\partial\psi}{\partial z}\right]_{h-}^{h+} = -2k\psi_1. \quad \text{(A10)}$$

However (A9) does not satisfy the boundary condition (A4). The total solution must include a zero PV component:

$$\psi = \psi_1 e^{\pm k(z-h)}e^{ik(x-ht)} + \psi_2(t)e^{-kz}e^{ikx}. \quad \text{(A11)}$$

Substitution in (A4), using $\psi_2(0) = 0$, gives

$$\psi_2(t) = \frac{h + c}{h - c}(e^{-ikht} - e^{-ikct})\psi_1, \quad h \neq c \quad \text{(A12)}$$
$$= -ik2hte^{-ikht}\psi_1, \quad h = c. \quad \text{(A13)}$$

The second term in (A12) is a neutral normal mode and (A13) shows that this is resonantly excited if its phase speed matches the speed of the PV anomaly.

For a general initial PV distribution in x, (but still the same δ-function in z), we may write the initial PV as a Fourier integral or sum of terms of the form (A7). The total solution is then a Fourier integral or sum of terms like (A11) with (A12). Even in a finite domain, the resonant wavelength is picked out. It is developed between the position of the PV perturbation $x = ht$ and the position determined by the group velocity, $x = 0$.

In dimensional terms, with h now the dimensional height at which the PV perturbation is included, the wavelength of the resonant neutral mode is $2\pi Nh/f$. The waves move at speed $h\Lambda$ with respect to the surface flow and a new trough or ridge is created every $t_c = \pi N/f_0\Lambda$.

In the solution shown in the text, the potential vorticity disturbance is composed of one wavelength of a sinusoid; this wavelength is $4Nh/f$. This is taken to be initially at the center of a large cyclic domain of length $60Nh/f$ and 64 wavenumbers are used in the Fourier decomposition. The solutions in Fig. 19 are shown for half the domain, up to $z = 3h$ and at time intervals $t_c/2$. Taking values for a frontal region:

$$f = 10^{-4}\,\text{s}^{-1}, \quad N^2 = 2.10^{-4}\,\text{s}^{-2}, \quad \Lambda = 2.10^{-2}\,\text{s}^{-1}$$
$$\text{and also} \quad h = 1\,\text{km}$$

gives the PV disturbance wavelength to be 570 km, the total domain length to be 8500 km, the resonant neutral mode wavelength 890 km, the time t_c between successive ridge and trough formation 6.2 h and the time between frames to be 3.1 h.

REFERENCES

Arakawa, A., and S. Moorthi, 1988: Baroclinic instability in vertically discrete systems. *J. Atmos. Sci.*, **45**, 1688–1707.

Bell, M. J., and A. A. White, 1988: Spurious stability and instability

in N-level quasi-geostrophic models. *J. Atmos. Sci.*, **45**, 1731–1738.

Bennets, D. A., and B. J. Hoskins, 1979: Conditional symmetric instability—a possible explanation for frontal rainbands. *Quart. J. Roy. Meteor. Soc.*, **105**, 945–962.

Bjerknes, J., 1919: On the structure of moving cyclones. *Geofys. Publikasjoner,* Norske Videnskaps-Akad. Oslo, **1**(2).

——, and H. Solberg, 1922: Life cycle of cyclones and the polar front theory of atmospheric circulation. *Geofys. Publ.,* Norske Videnskaps-Akad. Oslo, **3**(1).

Bosart, L. F., 1981: The Presidents' Day snowstorm of 18–19 February 1979: A subsynoptic-scale event. *Mon. Wea. Rev.*, **109**, 1524–1566.

Brown, J. A., 1969: A numerical investigation of hydrodynamic instability and energy conversions in the quasi-geostrophic atmosphere. Part I. *J. Atmos. Sci.*, **26**, 252–365.

Charney, J. G., 1947: The dynamics of long waves in a baroclinic westerly current. *J. Meteor.*, **4**, 135–162.

——, and M. E. Stern, 1962: On the stability of internal baroclinic jets in a rotating atmosphere. *J. Atmos. Sci.*, **19**, 159–172.

Cullen, M. J. P., and R. J. Purser, 1984: An extended Lagrangian theory of semigeostrophic frontogenesis. *J. Atmos. Sci.*, **41**, 1477–1497.

Duffy, D. G., 1976: The application of the semi-geostrophic equations to the frontal instability problem. *J. Atmos. Sci.*, **33**, 2322–2337.

Eady, E. T., 1949: Long waves and cyclone waves. *Tellus*, **1**, 33–52.

Edmon, H. J., B. J. Hoskins and M. E. McIntyre, 1980: Eliassen-Palm cross sections for the troposphere. *J. Atmos. Sci.*, **37**, 2600–2616. [See also Errata, *J. Atmos. Sci.*, **38**]

Eliasen, N. E., 1960: On the initial development of frontal waves. Publ. Danske Meteorol. Inst., Meddelser No. 13.

Emanuel, K., M. Fantini and A. J. Thorpe, 1987: Baroclinic instability in an environment of small stability to slantwise moist convection. Part I: Two-dimensional models. *J. Atmos. Sci.*, **44**, 1559–1573.

Farrell, B., 1982: The initial growth of disturbances in a baroclinic flow. *J. Atmos. Sci.*, **39**, 1663–1686.

——, 1984: Modal and nonmodal baroclinic waves. *J. Atmos. Sci.*, **41**, 668–673.

——, 1985: Transient growth of damped baroclinic waves. *J. Atmos. Sci.*, **42**, 2718–2727.

Harold, and Browning, 1969: The polar low as a baroclinic disturbance. *Quart. J. Roy. Meteor. Soc.*, **95**, 710–723.

Held, I. M., and B. J. Hoskins, 1985: Large-scale eddies and the general circulation of the troposphere. *Adv. Geophys.*, **28**, 3–31.

Hoskins, B. J., 1976: Baroclinic waves and frontogenesis Part I: Introduction and Eady waves. *Quart. J. Roy. Meteor. Soc.*, **102**, 103–122.

——, 1982: The mathematical theory of frontogenesis. *Ann. Rev. Fluid Mech.*, **14**, 131–151.

——, 1990: Dynamics of mid-latitude cyclones. *Extratropical Cyclones, Palmén Memorial Volume.* C. Newton, E. Holopainen, Eds, Amer. Meteor. Soc.

——, and F. P. Bretherton, 1972: Atmospheric frontogenesis models: Mathematical formulation and solution. *J. Atmos. Sci.*, **29**, 11–37.

——, and A. J. Simmons, 1975: A multi-layer spectral model and the semi-implicit method. *Quart. J. Roy. Meteor. Soc.*, **101**, 637–655.

——, and N. V. West, 1979: Baroclinic waves and frontogenesis. Part II: Uniform potential vorticity jet flows-cold and warm fronts. *J. Atmos. Sci.*, **36**, 1663–1680.

——, M. E. McIntyre and A. W. Robertson, 1985: On the use and significance of isentropic potential vorticity maps. *Quart. J. Roy. Meteor. Soc.*, **111**, 877–946.

——, and P. Berrisford, 1988: The storm of 15–16 October 1987: A potential vorticity perspective. *Weather,* **43**(3), 122–129.

Joly, A., and A. J. Thorpe, 1990a: Frontal instability generated by tropospheric potential vorticity anomalies. *Quart. J. Roy. Meteor. Soc.*, **116**, 525–560.

——, and ——, 1990b: The stability of time dependent flows: An application of fronts in developing baroclinic waves. *J. Atmos. Sci.*, **47**, in press.

——, and ——, 1990c: The stability of a steady horizontal shear front with uniform potential vorticity. *J. Atmos. Sci.*, **47**, in press.

Juckes, M. N., and M. E. McIntyre, 1987: A high resolution, one-layer model of breaking planetary waves in the stratosphere. *Nature,* **328**, 590–596.

Karoly, and B. J. Hoskins, 1982: Three dimensional propagation of planetary waves. *J. Meteorol. Soc. Jpn.*, **60**, 109–122.

Kleinschmidt, E., 1957: Dynamic meteorology. A. Eliassen, E. Kleinschmidt, Eds. *Handbuch der Physik.* Springer-Verlag, **48**, 112–129.

Kotchin, N., 1932: Über die stabilität von Marguleschen diskontinuitätsflächen. *Beitr. Phy. Atmos.*, **18**, 129.

Margules, 1906: Die energie der Stürm. *Meteorologishe Zeitschrift,* **23**, 481–497.

Matsumoto, S., S. Yoshizumi and M. Takeuchi, 1970: On the structure of the "Baiu-Front" and the associated intermediate scale disturbances in the low atmosphere. *J. Meteor. Soc. Jpn.*, **48**, 479–491.

McIntyre, M. E., 1970: On the non-separable baroclinic parallel-flow instability problem. *J. Fluid. Mech.*, **40**, 273–306.

Moore, G. W. K., and W. R. Peltier, 1987: Cyclogenesis in frontal zones. *J. Atmos. Sci.*, **44**, 384–409.

Orlanski, I., 1968: Instability of frontal waves. *J. Atmos. Sci.*, **25**, 178–200.

Pearce, R. P., 1978: On the concept of available potential energy. *Quart. J. Roy. Meteor. Soc.*, **104**, 737–755.

Petterssen, S., and S. Smebye, 1971: On the development of extratropical storms. *Quart. J. Roy. Meteor. Soc.*, **97**, 457–482.

——, D. L. Bradbury and K. Pedersen, 1962: The Norwegian cyclone models in relation to heat and cold sources. *Geophys. Norvegica,* **24**, 243–280.

Pierrehumbert, R. T., 1984: Local and global instability of zonally varying flow. *J. Atmos. Sci.*, **41**, 2141–2162.

Reed, R. J., and M. D. Albright, 1986: A case study of explosive cyclogenesis in the eastern Pacific. *Mon. Wea. Rev.*, **114**, 2297–2319.

——, A. J. Simmons, M. D. Albright and P. Undén, 1988: The role of latent heat release in explosive cyclogenesis: Three examples based on ECMWF operational forecasts. *Wea. Forecasting,* **3**, 217–229.

Sawyer, J. S., 1950: Formation of secondary depressions in relation to the thickness pattern. *Meteor. Mag.*, **79**, 1–5.

Schär, C., and H. Davies, 1990: An instability of mature cold fronts. *J. Atmos. Sci.*, **47**, 929–950.

Simmons, A. J., and B. J. Hoskins, 1976: Baroclinic instability on the sphere: Normal modes of the primitive and quasi-geostrophic equations. *J. Atmos. Sci.*, **33**, 1454–1477.

——, and ——, 1978: The life cycles of some nonlinear baroclinic waves. *J. Atmos. Sci.*, **35**, 414–432.

——, and ——, 1979: The downstream and upstream development of unstable baroclinic waves. *J. Atmos. Sci.*, **36**, 1239–1254.

——, and ——, 1980: Barotropic influences on the growth and decay of nonlinear baroclinic waves. *J. Atmos. Sci.*, **37**, 1679–1684.

Solberg, H., 1928: Integrationen der atmosphärischen Störungsgleichungen, *Geofys. Publikasjoner,* Norske Videnskaps-Akad. Oslo, **5**(9).

Staley, D. O., and R. L. Gall, 1977: On the wavelength of maximum baroclinic instability. *J. Atmos. Sci.*, **34**, 1679–1688.

Stone, 1966: On non-geostrophic baroclinic instability. *J. Atmos. Sci.*, **23**, 390–400.

Thorpe, A. J., and K. A. Emanuel, 1985: Frontogenesis in the presence of small stability to slantwise convection. *J. Atmos. Sci.*, **42**, 1809–1824.

Uccellini, L. W., P. J. Kocin, R. A. Petersen, C. H. Wash and K. F. Brill, 1984: The Presidents' Day cyclone of 18–19 February 1979: Synoptic overview and analysis of the subtropical jet streak influencing the pre-cyclogenetic period. *Mon. Wea. Rev.*, **112**, 31–55.

Valdes, P. J., and B. J. Hoskins, 1988: Baroclinic instability of the zonally averaged flow with boundary layer damping. *J. Atmos. Sci.*, **45**, 1584–1593.